

Distinct Regulation of Bioenergetics and Translation

by Group I mGluR and NMDAR

Sudhriti Ghosh Dastidar^{1,2}, Shreya Das Sharma^{1,3}, Sumita Chakraborty¹, Sumantra
Chattarji^{1,4}, Aditi Bhattacharya¹, Ravi S Muddashetty^{1,5} *

¹Institute for Stem Cell Sciences and Regenerative Medicine, Bangalore, India

²Manipal Academy of Higher Education, Manipal, India

³The University of Trans-Disciplinary Health Sciences and Technology, Bangalore, India

⁴ National Center for Biological Sciences, Bangalore, India

⁵ Lead Contact

Correspondence: ravism@instem.res.in

11
12
13
14
15
16
17
18
19
20
21
22
23
24
25
26
27

28

29

30

31 **Abstract:**

32 Neuronal activity is responsible for large energy consumption within the brain.

33 However, the cellular mechanisms draining ATP upon the arrival of a stimulus are yet

34 to be explored systematically at the post-synapse. Here we provide evidence that a

35 significant fraction of ATP is consumed upon glutamate stimulation to energize the

36 mGluR-induced protein synthesis. We find that both mGluR and NMDAR alter protein

37 synthesis and ATP consumption with distinct kinetics at the synaptic-dendritic

38 compartments. While mGluR activation leads to a rapid and sustained reduction in the

39 neuronal ATP level, NMDAR activation has no immediate impact on the same. ATP

40 consumption correlates inversely to the kinetics of protein synthesis for both the

41 receptors. We observe a persistent elevation in protein synthesis within 5 minutes of

42 mGluR activation and robust inhibition of the same within 2 minutes of NMDAR

43 activation, assessed by the phosphorylation status of eEF2 and metabolic labeling.

44 However, a delayed protein synthesis-dependent ATP expenditure ensues after 15

45 minutes of NMDAR activation. We identify a central role for AMPK in this correlation

46 between protein synthesis and ATP consumption. AMPK is dephosphorylated and

47 inhibited upon mGluR activation while it was rapidly phosphorylated upon NMDAR

48 activation. Perturbing AMPK activity disrupts the receptor-specific modulations of

49 eEF2 phosphorylation and protein synthesis. Therefore, our observations suggest that

50 the glutamate receptors required modulating the AMPK-eEF2 signaling axis to alter

51 neuronal protein synthesis and bioenergetics.

52

53 **Keywords:** mGluR, NMDAR, Protein synthesis, Bioenergetics, AMP-activated protein
54 kinase (AMPK).

55 **Short Summary:**

56 Stimulation of glutamate receptors induces robust protein synthesis within cortical neurons
57 and consumes a significantly large fraction of cellular ATP. Glutamate receptors viz. mGluR
58 and NMDAR modulate AMPK-eEF2 signaling uniquely leading to the dynamic regulation of
59 protein synthesis and bioenergetics.

60 **Key Highlights:**

- 61 • Protein synthesis following glutamate receptor activation is responsible for the bulk of
62 the activity-induced ATP consumption in cortical neurons.
- 63 • mGluR and NMDAR regulate protein synthesis with distinct kinetics and dictate the
64 subsequent impacts over neuronal ATP level.
- 65 • Dynamic modulation of AMPK and eEF2 phosphorylation is key to create unique
66 temporal features of receptor-specific protein synthesis and bioenergetics.

67 **Introduction**

68 The brain produces a significant energy burden within the body, even at the ‘resting’
69 state [1]. Further, the consumption of glucose or oxygen increases with brain
70 activation [2,3]. Within the brain, synapses are the sites of this ATP consumption
71 primarily [4,5] as several synaptic mechanisms are thought to give rise to an
72 exaggerated energy demand within a neuron [5]. Categorizing such mechanisms in
73 terms of their metabolic cost, however, has been difficult due to a lack of conclusive
74 evidence. Earlier studies based on theoretical calculations predicted that the largest
75 amount of ATP is expended to reestablish the ionic gradients following a neuronal

76 spike [5,6]. More recent work, however, demonstrated that the neuronal bursting is
77 quite energy-efficient [7]. Besides, the impact of the synaptic activity on the local
78 energy levels can be quite diverse as the energy supply may vary largely between
79 various neuronal compartments [8]. For example, recent reports have suggested that
80 the rapid endocytosis following glutamate release imposes the highest energy burden
81 at the pre-synaptic nerve terminals [9,10]. Besides, neuronal stimulation induces
82 abundant protein synthesis [11-13] the energy budget of which is still uncharted [14].
83 Protein synthesis is a determining resource for long-term synaptic plasticity [15-17]. It
84 is an energetically expensive procedure with a requirement of 4 ATP molecules for
85 each round of amino acid incorporation [14,18]. Activation of glutamate receptors
86 such as group I metabotropic glutamate receptors (mGluR) and NMDA Receptors
87 (NMDAR) are reported to alter the rate of protein synthesis [19-21] and are widely
88 implicated to facilitate or induce various forms of synaptic plasticity across different
89 brain regions [22-24].

90 Neurons meet the enhanced energy demand of activity by inducing ATP production
91 concomitantly. Activity-induced glycolysis, oxidative phosphorylation and the use of
92 glial metabolites like lactate for energy production is key to neuronal function and
93 survival [9, 13,25-27]. Yet, the link between the activity-induced protein synthesis
94 and energy homeostasis has remained unclear. A recent study, however, pointed out
95 that regulating AMP-activated protein kinase (AMPK) function is critical in maintaining
96 the synaptic ATP balance [25]. Considering the ability of AMPK to act as a metabolic
97 sensor, its competence to alter the catabolic-anabolic balance of the cell [28] and its
98 influence over various forms of synaptic plasticity [29,30], we predicted AMPK to

99 represent the missing link between protein synthesis and energy homeostasis. To test
100 the hypothesis, we asked the following questions: 1) How is the energy level altered
101 on neuronal stimulation? 2) How much of the consumed energy is allocated for
102 protein-synthesis? 3) How do the individual glutamate receptor subtypes generate
103 specific translation responses? And 4) How is the AMP Kinase activity regulated to
104 coordinate the translation and energy supply? Our observations suggest glutamate
105 stimulation in cortical neurons induces robust energy consumption due to the
106 activation of abundant protein synthesis. Both mGluR and NMDAR hold the ability to
107 modulate the AMPK-eEF2K-eEF2 signaling pathway to alter the kinetics of protein
108 synthesis.

109 **Results:**

110 **Protein Synthesis Results in a Significant Metabolic Burden Following Glutamate**
111 **Stimulation in Cortical Neurons:** To assess the impact of protein synthesis on cellular
112 energy content, we stimulated **high-density rat cultured cortical neurons** with
113 glutamate (25 μ M) for 5 minutes in the presence or absence of protein synthesis
114 inhibitors (anisomycin or cycloheximide) and quantified the ATP/(ATP+ADP) ratio from
115 cell lysates (**Figure 1A**). Glutamate stimulation led to a sharp drop in the neuronal
116 ATP/(ATP+ADP) ratio, a bulk of which was recovered significantly by pre-incubation
117 with anisomycin (25 μ M) or cycloheximide (350 μ M) (**Figure 1B** and **Figure EV 1D**)
118 suggesting a robust ATP consumption due to protein synthesis following the activation
119 of glutamate receptors. To identify the receptors responsible for protein synthesis
120 regulation, we repeated the glutamate stimulation in the presence or absence of D-
121 AP5 (25 μ M) + CNQX (40 μ M) (a combination of NMDA and AMPA receptor antagonists) or

122 MPEP (10 μ M) (mGluR5 antagonist). D-AP5 + CNQX treatment did not rescue the ATP
123 levels unless combined with anisomycin (**Figure 1C**). MPEP pre-treatment, however,
124 significantly rescued the energy drop following glutamate application (**Figure 1C**). To
125 verify this observation further, we stimulated cortical neurons with mGluR and NMDAR
126 specific agonists s-3,5 DHPG (50 μ M) and NMDA (20 μ M) respectively (**Figure EV 1A**) and
127 measured the ATP consumption. While DHPG addition led to a significant reduction in
128 the ATP/ATP+ADP ratio, NMDA treatment led to a modest yet not significant reduction
129 in the ATP level ($p=0.1501$), indicating that the mGluR activity is primarily responsible
130 for protein synthesis-dependent energy consumption on glutamate stimulation.

131 Since an optimal response to a stimulation depends on the spontaneous activity within
132 the neuronal network [31], we recorded the spontaneous neurotransmission at the
133 baseline of our high-density neuronal culture by whole-cell patch-clamp technique.
134 The resting membrane potential and other passive membrane properties such as
135 capacitance and input resistance values were comparable to previous reports (**Figure**
136 **EV 1I**) [32-35]. The neurons fired bursts of matured action potential spontaneously
137 detected both in the current-clamp and voltage-clamp mode (**Figure 1D and 1E**) at
138 day *in-vitro* 15. The action potential properties calculated through injecting a series
139 of 500ms depolarizing current steps (-40pA to +540pA) were comparable to previously
140 published reports (**Figure EV 1H, 1J, and 1K**) [33,34,36,37]. The presence of robust
141 mEPSCs recorded at the baseline supports the presence of spontaneous excitatory
142 neurotransmission (**Figure 1F and 1G**) [35]. Since the recording experiments were
143 done with different batches of cultures, we sought to verify our observations in figure
144 **1B** in the same batch of cultures used for recording experiments. As observed before,

145 glutamate addition led to a significant dip in the neuronal ATP/(ATP+ADP) ratio and
146 was significantly rescued upon anisomycin treatment (**Figure EV 1M**) arguing that the
147 observations presented in figure 1B and 1C were not the culture batch-specific
148 artifacts.

149 In these neuronal cultures, we further measured what percentage of energy is utilized
150 for endocytosis and ionic rebalancing as these are the two major mechanisms
151 proposed to present the bulk of the energy burden within the cell [5,9]. We used TTX
152 (1 μ M) to block the voltage-gated Na⁺ channels and small molecule inhibitors such as
153 Ouabain (1mM) and Dynasore (100 μ M) to understand the contribution of the Na⁺/K⁺
154 ATPase activity and endocytosis respectively. Surprisingly, Dynasore treatment did not
155 have a significant impact on glutamate-mediated energy usage (**Figure EV 1B and 1D**)
156 while Ouabain and TTX reduced the energy consumption only marginally (**Figure EV**
157 **1C and 1E**). These results argued that the energy burden of protein synthesis
158 outweighed that of the other mechanisms following neuronal activity.

159 We further examined the impact of mGluR and NMDAR stimulation individually on the
160 post-synaptic ATP content considering that distinct sets of factors regulate local and
161 global energy homeostasis within neurons [9]. For this, we prepared
162 synaptoneurosomes from 30 days old (P30) rat cortices and measured synaptic ATP
163 content on both the stimulations (**Figure 1H**). The ATP content was normalized to the
164 total protein content, in this case, to account for the variability between samples.
165 The significant enrichment of both pre-synaptic Synapsin 1 and post-synaptic PSD 95
166 proteins validated the preparation (**Figure 1I**). The synaptoneurosomes were also
167 enriched with ‘snowman’ shaped pre and post-synaptic conglomerate (**Figure EV 1F**)

168 [38] without a significant enrichment of glial protein GFAP (Figure 1I). In
169 synaptoneuroosomes, DHPG (100 μ M) treatment for 5 minutes led to a significant
170 reduction in the ATP level. MPEP and anisomycin pre-incubation, however, diminished
171 the effect of DHPG addition (Figure 1J and Figure EV 1G) as observed in Figure 1B
172 and 1C. 5 minutes of NMDA (50 μ M) stimulation contrarily, had no significant impact on
173 synaptic energy content (Figure 1K and Figure EV 1G). Therefore, mGluR dependent
174 reduction in the neuronal ATP level and the ability of anisomycin to rescue the dip
175 argue that protein synthesis shares the bulk of the glutamate-mediated energy
176 burden.

177 mGluR and NMDAR Impact Synaptic-dendritic ATP Levels with Distinct Kinetics

178 Since the glutamate receptors are concentrated on the dendritic spines [39], we
179 hypothesized that they may not only influence the rate of global protein synthesis
180 dynamically but may do so in a spatially distinct manner. We, therefore, monitored
181 the changes in the ATP/ADP ratio live using ratiometric sensor PercevalHR [40] until
182 15 minutes after DHPG and NMDA addition both at the soma and at the distal
183 dendrites ($\geq 50\mu$ m away from the soma) of cortical neurons plated at low-density
184 (Figure 2A-2C). Perceval pH bias was approximately corrected by simultaneous
185 measurement of intracellular pH and establishing a linear relation between Perceval
186 and pH-Red fluorescence as described previously [40,41] (Figure EV 2A). The low-
187 density cultured neurons had a reduced level of spontaneous neurotransmission due to
188 the lesser number of connections they formed [42-44] and showed reduced spiking
189 frequency with increasing current steps injected (Figure EV 1L). However, less
190 crowding within this kind of cell culture dishes allowed precise quantification of

191 ATP/ADP ratio within dendritic compartments using microscopy-based techniques. We
192 observed DHPG (50 μ M) application produced a significant and sustained drop in the
193 dendritic ATP/ADP ratio within 2 minutes while NMDA (20 μ M) application produced a
194 more delayed drop in the ratio after almost 10 minutes (**Figure 2C, 2E, and Figure EV**
195 **2B-2E**). To test the effect of protein synthesis inhibitors, we repeated both mGluR
196 and NMDAR stimulation in the presence of anisomycin. Not only did anisomycin
197 preincubation increase the baseline ATP level with time (**Figure EV 2F and 2G**), it
198 significantly rescued the stimulation-mediated dip in the ATP level within the
199 dendrites following the addition of both the stimuli (**Figure 2E and Figure EV 2C-2E**).
200 These observations suggest that inhibition of protein synthesis by anisomycin
201 increases the net ATP/ADP ratio of the cell. This gain in the ATP, however, can offset
202 the relatively smaller extent of ATP consumption by mechanisms other than protein
203 synthesis following glutamate receptor stimulation. To investigate the effect of
204 anisomycin treatment on the surface expression of glutamate receptors, we
205 quantified the cell surface level of mGluR5 and NR1 subunit of NMDAR in anisomycin
206 treated cortical neurons. The surface mGluR5 level remained unchanged on
207 anisomycin treated cells compared to basal untreated cultures while the NR1 surface
208 level was up-regulated on anisomycin treatment (**Figure EV 1L and 1M**). These
209 observations suggest that anisomycin pre-treatment does not reduce the surface level
210 of glutamate receptors and that the observed recovery of the ATP/ADP ratio on both
211 stimulations under anisomycin treated conditions was due to the inhibition of protein
212 synthesis. Surprisingly both the drugs had little or no impact within the soma (**Figure**
213 **2B and 2D and Figure EV 2B**) indicating a more dynamic energy utilization within

214 dendritic compartments compared to a more stable energy regulation at the soma
215 [45].

216 Since the steady-state ATP level is dependent on both the rate of production and
217 consumption, we tested whether glutamate stimulation perturbs the ATP production
218 and therefore leads to the observed drop in the neuronal ATP/ADP ratio. To verify,
219 we quantified the dendritic ATP/ADP ratio on glutamate stimulation in the presence
220 or absence of 2-deoxy glucose (2-DG, 30mM), a reversible inhibitor of glycolysis. In
221 neurons, glycolysis supports the baseline ATP level [9] and thus 2-DG preincubation
222 led to a significant decline in the basal dendritic ATP/ADP ratio (**Figure EV 2I and**
223 **2J**). However, 2-DG treatment did not alter the glutamate-mediated energy reduction
224 in the dendritic ATP/ADP ratio (**Figure EV 2K and 2L**) suggesting the observed effect
225 of glutamate stimulation is primarily because of ATP utilization and not because of
226 altered ATP synthesis.

227 Further, we verified the effect of mGluR and NMDAR stimulation on the kinetics of
228 ATP regulation at the mature synaptic compartments. We stimulated cortical
229 synaptoneuroosomes for a diverse period with DHPG and NMDA (1 min, 2 min, 5 min
230 and allowed recovery for 5 minutes post-stimulation) and quantified the ATP levels
231 (**Figure 2F and 1F**). As observed before, DHPG (100 μ M) addition rapidly decreased the
232 synaptic ATP level within 2 minutes, which returned to the baseline by 5 minutes of
233 recovery. Stimulation in the presence of anisomycin, however, failed to produce any
234 significant change in the synaptic ATP level (**Figure 2G**) suggesting a dynamic
235 alteration in protein synthesis creates a correlated change in the ATP level. NMDA
236 stimulation had no significant impact on the ATP level until 5 minutes, as observed in

237 dendrites (**Figure 2H, 2E and Figure EV 2H**). The effect of anisomycin preincubation
238 had a comparable effect to that of NMDA treatment alone (**Figure 2H and Figure EV**
239 **2H**) suggesting an absence of active protein synthesis immediately following NMDAR
240 stimulation. Together our observations establish that the well-correlated change in
241 neuronal protein synthesis and ATP content follows distinct kinetics upon mGluR and
242 NMDAR stimulation.

243 **mGluR and NMDAR Regulate eEF2 Phosphorylation to Create the Distinct Kinetics** 244 **of Protein Synthesis**

245 Since both NMDAR and mGluR impacted synaptic and dendritic ATP content
246 dynamically in a protein synthesis-dependent manner, we decided to study the
247 kinetics of *de-novo* protein synthesis following the addition of their specific agonists.
248 We quantified the amount of newly-synthesized proteins using FUNCAT metabolic
249 labeling based approaches as described previously [46]. Cortical neurons (DIV 15)
250 plated at low-density were stimulated with DHPG or NMDA for metabolic labeling and
251 the extent of labeling was quantified using mean fluorescence intensity which
252 proportionally correlated with the rate of protein synthesis throughout the labeling
253 period (**Figure 3A and 3B**). The absence of the FUNCAT signal in the control (without
254 AHA) verifies that the signal is specific to AHA labeled new proteins (**Figure EV 3A**).
255 We found that the DHPG application led to a significant elevation in the FUNCAT
256 intensity which sustained till 5 min of recovery compared to the time-matched
257 unstimulated control cultures (**Figure 3C, 3D, Figure EV 3A and 3B**). This
258 demonstrated that mGluR stimulation activates robust protein synthesis in cortical
259 neurons. In contrast, NMDA application caused a precipitous drop in the FUNCAT

260 intensity within 2 minutes compared to the time-matched unstimulated control
261 cultures. (**Figure 3C, 3D, Figure EV 3A and 3B**). We speculated that the observed
262 reduction in the FUNCAT intensity was because of protein degradation [47][48][49].
263 To investigate this, we repeated NMDA stimulation for 2 minutes in the presence of
264 MG132 (1 μ M), a 26s proteasome inhibitor that significantly improved the FUNCAT
265 intensity compared to cultures treated with NMDA alone. This supported our
266 hypothesis that a large-scale protein degradation ensues immediately following
267 NMDAR stimulation. NMDA treatment for 20 minutes, however, led to an abundant
268 increase in protein synthesis (**Figure EV 3C and 3D**) suggesting a dynamic modulation
269 of global protein synthesis.

270 Since translation can be regulated at multiple stages, we decided to focus on the
271 elongation regulation as elongation block is a viable mechanism to modulate
272 translation within a cell [50] and plays an important role in the context of NMDAR
273 mediated protein synthesis [21,51]. **The rate of ribosomal translocation can be**
274 **regulated by altering the phosphorylation of eEF2 [52]. Hyperphosphorylation eEF2 at**
275 **Thr⁵⁶ mediated by eEF2K reduces the rate of translation elongation [53-55].**
276 **Therefore, at any given instance, the status of eEF2 phosphorylation reflects an**
277 **integrated response from multiple biochemical pathways [21,56] and prompted us to**
278 **investigate the activity-dependent modulation of eEF2 phosphorylation through**
279 **immunolabeling 5 minutes after both mGluR or NMDAR stimulation in cortical neurons**
280 **(Figure 3E).** We observed a significant reduction in the p-eEF2 immunolabeling 5
281 minutes after DHPG treatment and a significant elevation in the immunolabeling 5
282 minutes after NMDA treatment compared to the time-matched unstimulated control

283 cultures (**Figure 3F**). This indicated that eEF2 phosphorylation was tuned to create
284 receptor-specific protein synthesis response and that at any given instance eEF2
285 phosphorylation reliably reflected the status of protein synthesis within a cell. Hence,
286 we used the phospho/total ratio of eEF2 as a readout for global translation in cortical
287 synaptoneurosomes (**Figure 3G and 3H**) and high-density cortical neurons (**Figure EV**
288 **3E and 3F**). Both synaptoneurosomes and neurons were stimulated for different
289 periods as mentioned before (**Figure 2F**). We observed that a significant difference
290 exists between the kinetics of how eEF2 phosphorylation was altered upon mGluR and
291 NMDAR stimulation (**Figure 3G and Figure EV 3F**). Comparison with the basal
292 condition revealed that mGluR stimulation led to an immediate and sustained
293 reduction in the phospho/total eEF2 ratio while NMDAR stimulation led to an
294 immediate increase in the ratio both in the synaptoneurosomes and in cultured
295 neurons. The phosphorylation status returned to the baseline by 5 mins of recovery in
296 both the cases (**Figure 3H and Figure EV 3E, 3F and 4A**). The temporally-matched
297 inverse correlation between FUNCAT signal and eEF2 phosphorylation implied that the
298 glutamate receptors had a strong influence over eEF2 to modulate protein synthesis
299 dynamically.

300 **Activity-dependent Dynamic Modulation of AMPK Is Necessary to Alter the eEF2** 301 **Phosphorylation:**

302 The phosphorylation of eEF2 is regulated by eEF2 Kinase which is known to be a
303 substrate for AMP-activated protein kinase [57]. AMPK is reported to sense the
304 intracellular AMP/ATP ratio or the ADP/ATP ratio and inhibits protein synthesis during
305 energy stress [28]. **Therefore, we sought to understand if the glutamate receptors**

306 needed to alter AMPK function to regulate protein synthesis. Since phosphorylation of
307 Thr¹⁷² is known to directly correlate with AMPK activation [58], we examined the
308 phosphorylation status of AMPK through immunolabeling 5 minutes after mGluR and
309 NMDAR stimulation in cortical neurons (**Figure 4A**). We observed a significant
310 reduction in the p-AMPK immunolabeling upon mGluR stimulation while an elevation
311 in the p-AMPK level following NMDAR stimulation compared to the time-matched
312 unstimulated control cultures (**Figure 4B**). This signified that the glutamate receptors
313 held the ability to modulate AMPK function following their activation. To verify
314 whether mGluR and NMDAR alter AMPK phosphorylation dynamically, we quantified
315 the phospho/total ratio of AMPK from cortical synaptoneuroosomes after various
316 periods of DHPG or NMDA treatment (**Figure 4C**). We observed a persistent and
317 significant reduction in the phospho/total ratio of AMPK within 2 minutes of DHPG
318 application compared to unstimulated synaptoneuroosomes (**Figure 4D and Figure EV**
319 **4A**). Surprisingly, DHPG mediated reduction in AMPK phosphorylation was reversed in
320 the presence of anisomycin (**Figure 4C, 4D and Figure EV 4B**) indicating that the
321 AMPK activity is regulated in turn by the newly synthesized proteins involving a
322 feedback-inhibition. We speculated, therefore, that the synthesis of any AMPK
323 specific phosphatase could explain the dephosphorylation of AMPK.

324 While the exact identity of the AMPK phosphatase is still elusive [59-61], we chose to
325 investigate the role of α -SNAP, an AMPK specific inhibitor [61], in the context of
326 mGluR stimulation in cortical synaptoneuroosomes (**Figure 4E**). We observed a
327 significant elevation in the α -SNAP level within 1 minute of DHPG addition, which was
328 absent in the anisomycin treated preparations (**Figure 4F**). The activity-induced

329 changes in α -SNAP level inversely correlated with the kinetics of AMPK activation
330 (**Figure 4D**) suggesting that α -SNAP plays a critical role in dictating the status of AMPK
331 activity upon mGluR stimulation. We sought to confirm the role of α -SNAP with two
332 approaches. First, we quantified the colocalization between α -SNAP and AMPK, which
333 increased modest yet significantly on mGluR stimulation in low-density cultured
334 neurons (**Figure 4G and 4H**). Second, we acutely knocked down the α -SNAP protein
335 level using the siRNA-based approach and quantified the p-AMPK levels in the neurons
336 (**Figure 4I**). The α -SNAP siRNA treatment did not alter the p-AMPK level significantly
337 on the basal condition while it led to a marked reduction in the α -SNAP protein level
338 compared to scrambled siRNA treated cultures (**Figure EV 4C**). However, α -SNAP-
339 siRNA treatment eliminated the DHPG induced reduction in the AMPK phosphorylation
340 (**Figure 4J**) indicating a more complex regulation of AMPK. Our observations also
341 argue that the recruitment of α -SNAP for the AMPK regulation is an exclusive feature
342 of the mGluR mediated signal transduction.

343 **NMDAR Regulates AMPK Activity in a Ca²⁺ Dependent Manner**

344 The fact that NMDAR stimulation led to an up-regulation of the p-AMPK level (**Figures**
345 **4A and 4B**) and that AMPK is a known substrate of CamKKIIB [62], made us wonder
346 whether the entry of extracellular Ca²⁺ through open NMDAR channels regulates AMPK
347 phosphorylation. We first decided to investigate the status of the AMPK
348 phosphorylation following various periods of NMDA incubation (**Figure 5A**). We
349 observed a rapid and persistent increase in the phospho/total ratio of AMPK within 1
350 minute of NMDA addition (**Figure 5B**) corroborating our previous observation in **Figure**
351 **4B**. We confirmed the role of Ca²⁺ by repeating the stimulation in the absence of

352 extracellular Ca^{2+} , which eliminated the NMDAR dependent elevation of the
353 phospho/total ratio of AMPK (**Figure 5B**). Besides, the NMDAR mediated increase in
354 the phospho/total ratio of eEF2 was diminished significantly in the absence of
355 extracellular Ca^{2+} indicating AMPK and eEF2 phosphorylations were altered in a
356 correlated fashion on NMDAR stimulation with Ca^{2+} playing a critical role in dictating
357 the kinetics (**Figure EV 4E and 4F**). We sought to verify the NMDA dependent Ca^{2+}
358 entry by live monitoring the cytosolic free Ca^{2+} following NMDA addition in the low-
359 density cultured neurons using the Fluo-8AM probe. We observed a rapid and
360 persistent increase in Fluo8 fluorescence on NMDA addition (**Figure 5C**) indicating an
361 increase in the cytosolic Ca^{2+} concentration on NMDA treatment. The rise in Fluo8
362 fluorescence could be reversed by D-AP5 or MK801 pre-incubation for 30 minutes
363 (**Figure 5D, 5E, and Figure EV 4D**) arguing the response was NMDAR specific. A
364 further increase in fluorescence on ionomycin addition in the presence of 10mM Ca^{2+}
365 provided the fluorescence maxima for each cell (**Figure 5D**). The elevation in
366 fluorescence was significantly reduced in the absence of extracellular Ca^{2+} (**Figure**
367 **5D, 5E, and Figure EV 4D**) indicating that a large amount of extracellular Ca^{2+} enters
368 the cell upon NMDA addition. This elevation in cytosolic free Ca^{2+} activated AMPK in
369 response to stimulation possibly by engaging CamKKIIB [51,63]. Interestingly, we
370 observed a similar extent of elevation in the phospho/total ratio of eEF2 on NMDAR
371 stimulation in cortical synaptoneurosomes both in the presence or absence of
372 extracellular Mg^{2+} , an ion that occludes the NMDAR channel pore (**Figure EV 4G**).
373 Together these results suggested that NMDA addition led to an abundant Ca^{2+} entry

374 through the open channels of synaptic NMDAR, regulating both AMPK and eEF2
375 phosphorylation within the neuron.

376 Acute Perturbation of AMPK Disrupts the Receptor-specific Translation Response

377 The link between the AMPK regulation and glutamate receptor-mediated protein
378 synthesis in cortical neurons prompted us to investigate whether the AMPK regulation
379 was necessary to generate the receptor-specific protein synthesis response. We
380 probed this question using two independent approaches. To begin with, we repeated
381 the mGluR stimulation in the presence of 5-aminoimidazole-4-carboxamide
382 ribonucleotide (AICAR; 1mM) which is known to activate AMPK acutely [64] (**Figure**
383 **6A**). We observed AICAR pre-treatment for 1 hour led to a significant elevation in p-
384 eEF2 levels (**Figure 6C, Figure EV 4H**) without affecting the FUNCAT signal (**Figure**
385 **6D, Figure EV 4H**) basally in the low-density cortical neurons. However, AICAR
386 treatment significantly rescued the DHPG induced reduction in p-eEF2 levels (**Figure**
387 **6A, B, Figure EV 4H**) and eliminated the DHPG induced rise in the FUNCAT intensity
388 (**Figure 6C, D, Figure EV 4H**). This meant that the acute apriori activation of AMPK
389 disrupts the mGluR-mediated dephosphorylation of eEF2 and a subsequent elevation
390 in protein synthesis. Similarly, we examined the impact of AMPK activation on NMDAR
391 mediated protein synthesis regulation. We stimulated cortical neurons with NMDA in
392 the presence of compound C (Dorsomorphin/CC), a small molecule inhibitor of AMPK
393 (**Figure 6E**). CC pre-treatment for 1 hour had no significant impact on p-eEF2 levels
394 (**6F, Figure EV 4H**) but led to a significant increase in the FUNCAT intensity (**6G,**
395 **Figure EV 4H**). However, CC abolished the NMDA mediated rise in p-eEF2 levels
396 (**Figure 6F**) and significantly rescued the inhibition of protein synthesis (**Figure 6G**).

397 Therefore, acute inhibition of AMPK perturbed the NMDA mediated
398 hyperphosphorylation of eEF2 and inhibition of global protein synthesis. These also
399 confirmed the pivotal role of AMPK in dictating the fate of global protein synthesis
400 following glutamate receptor activation.

401 **Discussion:**

402 In our work, we demonstrate that the activity-mediated protein synthesis in response
403 to mGluR and NMDAR stimulation leads to distinct and dynamic alterations of the
404 neuronal energy level. A unique combination of AMPK-eEF2 signaling brings about the
405 characteristic changes in protein synthesis specific for each stimulus.

406 **Protein Synthesis Consumes Bulk of the Energy on Glutamate Stimulation in** 407 **Neurons**

408 Protein synthesis is essential for axonal path finding [65], axonal and dendritic
409 branching [66,67] synaptic plasticity [68,69] and other neuronal functions. Our study
410 establishes protein synthesis to have a major contribution to activity-mediated energy
411 consumption. However, it would be interesting to delineate whether any secondary or
412 tertiary mechanism activated following protein synthesis is responsible for any
413 fraction of this consumption. Strategies allowing the synthesis of non-functional
414 proteins using genetically incorporated un-natural amino acids can assist in addressing
415 this issue [70]. Our observation also suggests that the energetic cost Na^+/K^+ ATPase is
416 **less than protein synthesis unlike predicted earlier** [5]. Though vesicle endocytosis is
417 known to cause the major energy drainage at the presynaptic nerve terminals, we did
418 not observe any significant contribution originating from it at the post-synaptic
419 compartments [9]. Our observations, however, demand further exploration of the

420 energy consumption by other activated synaptic mechanisms such as organellar
421 movement, cytoskeletal rearrangement, autophagy, global protein degradation and
422 others [5,71].

423 **mGluR and NMDAR Affect the Rate of Global Translation**

424 Results from our work also reveal that mGluR dependent protein synthesis follows
425 distinct kinetics as compared to that of NMDAR. The kinetics of protein synthesis was
426 inversely correlated with the kinetics of ATP consumption. Group I mGluR have been
427 widely reported to activate protein synthesis [19,20,72] across various brain regions
428 [73-75]. Our results indicate that mGluR mediated translation activation produced a
429 rapid reduction in the synaptic-dendritic ATP level. However, the somatic ATP level
430 remained unchanged on mGluR stimulation even though protein synthesis was
431 activated in the cell body (Figure 3C and 3D). This implies that the impact of protein
432 synthesis on the steady-state ATP level depends on how rapidly the local energy
433 supply pathways compensate for the enhanced energy demand within a neuronal
434 compartment [8,76]. In contrast, NMDAR stimulation led to a biphasic protein
435 synthesis response with an early inhibition and a delayed activation phase [21]. It is
436 interesting that unlike the effect of anisomycin (Figure EV 2F and 2G), NMDAR
437 mediated inhibition of protein synthesis did not elevate the cellular ATP level and
438 only produced a delayed reduction of the same. This is probably because of the ATP
439 consumed for large scale protein degradation [77] (Figure EV 3D) offsets the gradual
440 build-up of ATP upon protein synthesis inhibition (Figure EV 2G).

441 **The role of AMPK-eEF2 Signaling to Create Differential Response to mGluR and** 442 **NMDAR Stimulation**

443 Our results also emphasize the key role of AMP-activated protein Kinase in both
444 mGluR and NMDAR mediated translation regulation. Previously, AMPK has been
445 demonstrated to regulate activity-induced energy metabolism [25], sustained activity-
446 induced GLUT4 membrane expression in nerve terminals [78] and various forms of
447 synaptic plasticity [29,30]. Our current observations, however, establish AMPK as a
448 mechanistic link to coordinate activity-induced protein synthesis and energy
449 metabolism. AMPK inhibits global protein synthesis by activating eEF2 Kinase directly
450 or via indirect mechanisms [79]. mGluR mediated AMPK inhibition, therefore, allows
451 the dephosphorylation of eEF2 causing an enhanced protein synthesis. We found that
452 α -SNAP, one of the proteins synthesized on mGluR stimulation, inhibited AMPK likely
453 through its phosphatase activity [61] suggesting there exist several noncanonical
454 mechanisms to regulate AMPK within neurons. Also, it would be interesting to
455 understand the contribution of other AMPK phosphatases like PP2A in governing the
456 course of mGluR-induced signaling and protein synthesis [80]. NMDAR stimulation, on
457 the contrary, led to immediate activation of AMPK in a Ca^{2+} dependent manner
458 probably by recruiting the upstream CamKKIIB. The activated AMPK, in turn, led to
459 hyperphosphorylation of eEF2 (**Figure EV 4D**) resulting in an inhibition of neuronal
460 protein synthesis as observed before [51].

461 In summary, our study demonstrates the striking influence of protein synthesis on the
462 synaptic-dendritic energy homeostasis following the stimulation of glutamate
463 receptors. AMPK plays a pivotal role in dictating this **correlation (Figure 6H)**. It would
464 be intriguing, however, to elucidate how the correlation is altered in
465 neurodevelopment and various pathophysiological conditions such as stroke, epilepsy

466 or neurodegenerative diseases. The study may also help in identifying potential
467 therapeutic targets for diseases involving bioenergetic impairments and dysregulated
468 protein synthesis.

469

470

Materials and Methods

471 **Ethics Statement:** All animal work was done in compliance with the procedures
472 approved by the Institutional Animal Ethics committee (IAEC) and the Institutional
473 Biosafety Committee (IBSC), InStem, Bangalore, India. All rodent work was done with
474 Sprague Dawley (SD) rats. Rats were kept in 20-22°C temperature, 50-60% relative
475 humidity, 0.3µm HEPA filtered air supply at 15-20 ACPH and 14/10 light/dark cycle
476 maintained. Food and water were provided *ad libitum*.

477 **Antibodies, Drugs, and Other Reagents:** Anti-phospho eEF2 antibody (Thr 56; cat no:
478 2331; Used at 1:1000 dilution for western blotting analysis and 1:250 for
479 immunocytochemistry), anti-eEF2 antibody (cat. no 2332; Used at 1:1000 dilution for
480 western blotting analysis), anti-phospho AMPKα antibody (Thr 172; cat. no: 2535; used
481 at 1:500 dilution for western blotting analysis and 1:100 for immunocytochemistry
482 analysis) and anti-AMPK antibody (cat no: 2532; used at 1:1000 dilution for western
483 blotting analysis) were obtained from Cell Signaling Technologies (MA, US). Anti-
484 tubulin antibody (cat no: T9026; used at 1:1000 dilution for western blotting analysis),
485 anti-MAP2B antibody (cat no: M9942; used at 1:500 dilution for
486 immunocytochemistry), anti-rabbit HRP labeled secondary antibody (cat no: A0545;
487 used at 1:5000 dilution for western blotting analysis) and anti-mouse HRP labeled
488 secondary antibody (cat no: A9044; used at 1:5000 dilution for western blotting

489 analysis) were obtained from Sigma-Aldrich (St. Louis, MO). Anti-rabbit secondary
490 antibody Alexa 555 labeled (cat no: A11032; used at 1:500 dilution for
491 immunocytochemistry), anti-mouse secondary antibody Alexa 488 labeled (cat no:
492 A11008; used at 1:500 dilution for immunocytochemistry) and α -SNAP (NAPA) siRNA
493 were obtained from Thermo Fisher Scientific (Waltham, MA). Anti- α -SNAP antibody
494 (cat no: X1026; used at 1:1000 dilution for western blotting analysis) was obtained
495 from Exalpa Biologicals. Anti-Synapsin 1 antibody (cat no: ab64581, Used at 1:1000
496 dilution for western blotting) was obtained from Abcam (Cambridge, UK). Glutamate
497 (25 μ M), NMDA (20 μ M for neurons and 40 μ M for SNS), CNQX (40 μ M), Anisomycin (25 μ M
498 for neurons and 50 μ M for synaptoneurosomes), Cycloheximide (100 μ g/ml), Ouabain
499 octahydrate (1mM), Dynasore hydrate (100 μ M), Poly-L-Lysine (0.2mg/ml), Pluronic-F-
500 127(0.002%), BAPTA (10mM), Ionomycin (10 μ M), 2 deoxy-glucose (30mM) and
501 oligomycin A (2.5 μ M) were obtained from Sigma-Aldrich (St. Louis, MO). S-3,5 DHPG
502 (20 μ M for neurons and 100 μ M for SNS), 5-aminoimidazole-4-carboxamide
503 ribonucleotide (AICAR, 1mM), D-AP5 (25 μ M), MK-801 (10 μ M), MPEP (10 μ M),
504 Tetrodotoxin citrate [TTX, 1 μ M for measuring (ATP/ATP+ADP) and 0.5 μ M for
505 **electrophysiology experiments**] were obtained from Tocris Biosciences. Compound C
506 (dorsomorphin; 40 μ M in synaptoneurosomes and 20 μ M in cultured neurons) were
507 obtained from Santa Cruz Biotechnology (Santa Cruz, CA). Fluo-8 AM (2 μ M) was
508 obtained from AAT Bioquest (Sunnyvale, CA). FUGW-PercevalHR was a gift from Gary
509 Yellen (Addgene plasmid # 49083; <http://n2t.net/addgene>: 49083; RRID:
510 Addgene_49083). GW1-pHRed was a gift from Gary Yellen (Addgene plasmid # 31473;
511 <http://n2t.net/addgene>: 31473; RRID: Addgene_31473).

512 **Synaptoneurosome Preparation:** Synaptoneurosomes were prepared from SD WT rat
513 cortices at the age between post-natal day 28-33 (P28-33) following differential
514 centrifugation method as described previously [21,81,82]. Briefly, rat cortices were
515 dissected and homogenized at 4°C in 8 volumes of synaptoneurosome (SNS)
516 homogenization buffer [containing (in mM) 25 Tris-HCl pH 7.4, 118 NaCl, 4.7 KCl, 1.2
517 MgSO₄, 2.5 CaCl₂, 1.53 KH₂PO₄, and 212.7 glucose, supplemented with Complete
518 protease inhibitors (Roche)]. Homogenates were then passed through three 100µm
519 nylon mesh filters followed by one 11µm filter MLCWP 047 Millipore (Bedford, MA) and
520 centrifuged at 1000g for 20 minutes at 4°C. The pellet was resuspended into 2ml of
521 the same buffer. In experiments with no Ca²⁺, CaCl₂ was removed from the
522 resuspension buffer. The resuspended SNS particles were then incubated at 37°C to
523 regain active metabolism.

524 **Synaptoneurosome Stimulation:** For Stimulation, synaptoneurosomes were pre-
525 warmed at 37°C for a minimum of 5 minutes. A sample fraction aliquoted at this point
526 was considered as the unstimulated condition or 0 min of stimulation for further
527 analysis. This was followed by Gp I mGluR and NMDAR stimulation with specific
528 agonists (s)3,5-dihydroxyphenylglycine (DHPG; 100µM) and N-methyl D-aspartate
529 (NMDA; 40µM) respectively. Further fractions were collected after 2 minutes and 5
530 minutes of stimulation. A fraction was collected 5 minutes post-stimulation (5 min
531 stimulation + 5 min recovery). For this, the synaptoneurosomes were first stimulated
532 for 5 minutes with agonists. This is followed by the removal of the stimulus through
533 centrifugation at 13,000g for 20 seconds and resuspension with 37°C pre-warmed
534 synaptoneurosome homogenization buffer. These synaptoneurosomes were further

535 incubated for 5 minutes and processed for ATP measurement, protein estimation, and
536 western blot analysis. For ATP measurements, stimulation was terminated by direct
537 lysis of synaptoneurosomes with an equal volume of boiling water [83]. This was
538 followed by centrifugation at 20,000g for 2.5 minutes for the measurement of soluble
539 ATP content from the supernatant. For protein estimation and western blot analysis,
540 synaptoneurosomes fractions were centrifuged at 13,000g for 20 seconds followed by
541 lysis with lysis buffer [containing: 50 Tris-Cl (pH-7.4), 150 NaCl, 5 MgCl₂, 1% Triton-X-
542 100, supplemented with EDTA free protease inhibitor complex (Sigma, cat. no. S8830)
543 and phosphatase inhibitor cocktail (Roche, ref.no. 04906837001)] (**Stimulation
544 protocol figure 2F**). In experiments involving pre-treatment of drugs, the
545 preincubation period varied depending on the drugs, which were directly added after
546 the resuspension step. Untreated control synaptoneurosomes were pre-incubated for
547 the same period as drug pre-treatment time for comparisons.

548 **Cell Line and Primary Neuronal Culture:** Primary neurons were cultured from
549 cerebral cortices as described by Banker & Goslin, 1998 [84]. Embryos were obtained
550 from females on the 18th day of the gestation period (E18) and cerebral cortices were
551 dissected out in ice-cold Hank's balanced salt solution under a dissection microscope.
552 Cells were dissociated with 0.25% trypsin solution at 37 °C for 10 minutes followed by
553 mechanical trituration in minimal essential medium (MEM, Thermo fisher) with 10%
554 fetal bovine serum (Sigma). Dissociated cells were plated on tissue culture dishes or
555 coverslips coated with poly-L-lysine (0.2 mg/ml in borate buffer, pH 8.5). Neurons
556 were attached to the substrate in MEM with 10% FBS for 3h, followed by defined
557 Neurobasal Medium (Invitrogen) with GlutaMAX™ supplement (Gibco™) and B-27

558 supplements (Invitrogen) for 15 days at 37°C in a 5% CO₂ environment. For
559 immunocytochemistry, cells plated on coverslips kept in a 10cm diameter tissue
560 culture dish with a plating density of 10⁵ cells/dish. The coverslips are then inverted
561 onto an astroglial bed in neurobasal media after substrate attachment in MEM. For
562 biochemical and immunoblotting experiments, cells were grown on 6 well dishes or
563 35mm diameter dishes, for live imaging cells were plated on 35mm diameter glass-
564 bottom dishes, for immunolabeling cells were plated on 15mm diameter glass
565 coverslips with 0.15mm thickness. The plating density used for various assays are as
566 follows: ATP:ADP Ratio (Biochemical)- 4X10⁴ /Cm² (High-density); ATP:ADP (Imaging)-
567 2X10⁴ /Cm² (Low-density); Western blotting of eEF2- 4X10⁴ /Cm² (High-density);
568 FUNCAT, immunolabeling and Ca²⁺ Assay (Imaging)- 2X10⁴ /Cm² (Low-density); KD of α-
569 SNAP and Western Blotting- 4X10⁴ /Cm² (High-density).

570 **Electrophysiology:** To test the functionality of the rat cortical neurons whole-cell
571 patch-clamp recordings were performed as previously described [85,86]. Rat cortical
572 neurons were cultured on glass coverslips and transferred onto the recording chamber
573 after 14-15 days *in vitro*. An extracellular solution composed of the following (in mM)
574 NaCl 152, KCl 2.8, HEPES 10, CaCl₂ 2, glucose 10, pH 7.3 - 7.4 (300 - 320 mOsm) was
575 constantly perfused using a peristaltic pump (Watson - Marlow, Wilmington,
576 Massachusetts, USA). Patch pipettes (3 - 4 MΩ resistance, ≈ 2 μm tip diameter) were
577 pulled from thick-walled Borosilicate glass using a P1000 horizontal micropipette
578 puller (Sutter Instruments, Novato, California, USA. For current-clamp recordings
579 pipettes were filled with an internal solution consisting of the following (in mM) : K-
580 gluconate 155, MgCl₂ 2, Na- HEPES 10, Na-PiCreatine 10, Mg₂-ATP 2 and Na₃-GTP 0.3,

581 pH 7.3 (280 - 290 mOsm) and Cesium gluconate 110, CsCl 20, Na- HEPES 10, NaCl 4,
582 QX 314 5, EGTA 0.2, Na-PiCreatine 10, Mg₂-ATP 2 and Na₃-GTP 0.3, pH 7.3 (280 - 290
583 mOsm) was used for voltage-clamp recordings. Signals were filtered at 3 kHz and 10
584 kHz for voltage and current clamp, respectively, using a Multiclamp 700B amplifier
585 and digitized at 10 kHz with Axon Digidata 1550 (Molecular Devices, Union City,
586 California, USA). Holding current was less than 100 pA for all the recordings and the
587 series resistance R_s was less than 30 MΩ. Experiments, where R_s drifted by more than
588 25%, were discarded. In action potential (AP) recordings, neurons were held at -60 mV
589 and a series of depolarizing current pulses (-40 pA to +540 pA, 500 msec) were
590 injected. AP parameters were analyzed from the first action potential using Clampfit
591 10.5 (pClamp, Molecular Devices, Union City, California, USA, RRID: SCR_011323). For
592 recording miniature excitatory postsynaptic currents (mEPSC) in the voltage-clamp
593 mode neurons were held at -70mV in the presence of 0.5 μM TTX (Hello Bio, Bristol,
594 UK) and recorded for 5 min of which the last 1 min was used to analyze the mEPSC
595 parameters. For spontaneous burst recordings in both voltage and current clamp, the
596 neurons were clamped at -70 mV and recorded for 5 min. Burst number was defined
597 as the average number of bursts in 5 min and burst duration was calculated as the
598 time interval between the start of membrane depolarization to the end of
599 depolarization. All values are expressed as mean ± SEM. Each data set was tested for
600 normality using the D'Agostino & Pearson test. Column statistics was performed for
601 calculating the mean, standard deviation, and SEM. All the statistical tests were
602 performed using GraphPad (GraphPad Software Inc., La Jolla, California, USA, RRID:
603 SCR_002798).

604 **Metabolic Labeling:** For metabolic labeling of proteins, neurons were incubated for 1
605 hour in methionine-free Dulbecco's Modified Essential Medium (DMEM, Thermo
606 Fisher). This was followed by the addition of L-azidohomoalanine (AHA; 1 μ M) for the
607 next 55 minutes in the same medium. At this point, a group of cells were fixed with
608 4% Paraformaldehyde (PFA) for 20 minutes and would be considered as unstimulated
609 basal for further analysis. This was followed by either fixing the cells with 4% PFA or
610 the cells were stimulated with mGluR and NMDAR specific agonists DHPG (50 μ M) and
611 NMDA (20 μ M) respectively for 2 minutes, 5 minutes or post-stimulation 5 minutes
612 recovery (5 min stim + 5 min recovery) and subsequently fixed with 4% PFA. Cells
613 were then permeabilized in TBS50 [containing (in mM):50 Tris-Base, 150 NaCl] + 0.3%
614 Triton X 100 solution and blocked using TBS50 + 0.1% Triton X 100 + 2% BSA + 4% FBS
615 containing blocking solution. Newly synthesized proteins were then labeled with
616 Alexa-Fluor-555-alkyne [Alexa Fluor 488 5-carboxamido-(propargyl), bis
617 (triethylammonium salt)], by allowing the fluorophore alkyne to react with AHA azide
618 group through click chemistry. All reagents were from Thermo Fisher and
619 stoichiometry of reagents were calculated according to the suggested manual by the
620 manufacturer (CLICK-iT cell reaction buffer kit, cat.no. C10269). Signal intensity was
621 then measured using confocal microscopy to calculate the amount of newly
622 synthesized proteins. For the detection of neurons, MAP2B immunolabeling was used.

623 **Immunocytochemistry:** Rat primary cortical neurons were stimulated with either
624 50 μ M DHPG or 20 μ M NMDA for 5mins. Cells were fixed with 4% PFA and processed for
625 imaging as described before. In brief, cells were permeabilized using TBS50 + 0.3% T
626 solution and were treated with Tris-Glycine solution (containing in Moles: 0.5 Tris-

627 base and 0.2 Glycine) before blocking with blocking buffer [TBS50 + 0.1% T) + 2% BSA
628 + 4% FBS]. Primary antibodies were incubated in blocking buffer overnight at 4 °C
629 under gentle shaking conditions followed by washes. Alexa Fluor 488 coupled anti-
630 mouse and Alexa Fluor 555 coupled anti-rabbit secondary antibodies were incubated
631 for 2h at room temperature. Finally, coverslips were mounted for imaging using
632 Mowiol® 4-88 mounting media. Images were acquired on a Leica TCS SP5 confocal
633 microscope (Leica Biosystems) with HCX PL APO 63X, NA 1.4, oil immersion objective.
634 Imaging conditions were kept constant across groups. Images were acquired on
635 Olympus FLUOVIEW 3000 confocal laser scanning microscope (Olympus Corporation)
636 with HCX PL APO 60x, NA 1.4, oil immersion objective. For the quantification of
637 fluorescence intensities, images were acquired while keeping the open pinhole
638 configuration to collect lights from planes below and above the focal plane as well.
639 The objective was moved in the Z direction with a step size of 0.5µm for 12 such
640 steps to ensure the light was collected from the entire cell across its thickness. For
641 quantification of colocalization, images were acquired using 2.5x optical zooming to
642 satisfy Nyquist's sampling theorem of information theory for maximum resolution in
643 the XY direction. The pinhole was kept at 1 Airy unit to ensure optimum resolution
644 and confocal stacks were acquired with a step size of 0.3µm calculated based on the
645 fluorophore wavelength. Imaging conditions were kept constant across different data
646 sets, across experiments.

647 **Live Cell Fluorescence Microscopy:**

648 **Imaging Dendritic ATP/ADP Ratio:** Cells were imaged on Zeiss LSM 780 confocal laser
649 scanning microscope (Carl Zeiss, Oberkochen, Germany) with 63X Zeiss plan-

650 apochromatic oil immersion objective, NA 1.4 with argon lasers of specified
651 wavelengths. Cells were grown in Neurobasal media containing B27 supplements and
652 Glutamax and were transfected with PercevalHR and pH-Red construct for
653 simultaneous monitoring of intracellular ATP/ADP ratio and pH. pH monitoring was
654 done as suggested in previous studies (56) to correct for the bias created in Perceval
655 HR fluorescence solely due to the change in intracellular pH. Perceval HR was excited
656 with 488/20 nm and 405/20 nm band-pass filters and emissions were collected
657 through a 520/15nm band-pass filter. Excitation and emission beams were separated
658 through a 490 nm short pass dichroic mirror. pH-Red was excited using 561/20nm and
659 455/10 nm band-pass filters and emissions were collected through a 630/50 nm band-
660 pass filter. A 560 nm short-pass dichroic was used to separate excitation and emission
661 beams.

662 Neurons were imaged at room temperature in 37°C pre-warmed Neurobasal media
663 without phenol red (Thermo Fisher, Waltham, MA, USA) containing 15mM HEPES. For,
664 approximate pH bias removal, the linear relationship established between Perceval
665 HR and pH-Red fluorescence for the high glucose ‘ATP Loaded’ state by Tantama et.
666 Al., 2014 [40] was used. The relationship was used to predict the pH bias of the
667 Perceval HR signal from the continuously monitored pH-Red signal and was normalized
668 to the observed Perceval HR fluorescence for the entire period of the experiment.
669 Images were captured at a 16-bit image format with 512X512 pixel distribution with a
670 frame rate of 1 per 15 seconds.

671 **Ca²⁺ Imaging:** Growth media from cells grown on glass-bottom Petri dishes were first
672 removed and were washed with imaging media [containing in mM: 120 NaCl, 3 KCl, 2

673 CaCl₂, 1MgCl₂, 3 NaHCO₃, 1.25 NaH₂PO₄, 15 HEPES, 30 glucose (pH 7.4). They were
674 incubated with 2 ml freshly prepared dye solution (2 μM Fluo-8 AM and 0.002%
675 Pluronic F-127 in imaging media) at 37°C for 10 mins followed by a 5 minutes
676 incubation procedure at the same temperature with the imaging media. They were
677 then imaged on Olympus FV3000 confocal laser scanning inverted microscope with 20X
678 air objective lens NA 0.75, illuminated with 488nm solid-state lasers. Images were
679 acquired at a rate of single frame per 3.22s intervals at room temperature. Cells were
680 imaged for 322 sec (100 frames) for recording spontaneous activity, followed by 644
681 sec (200 frames) with stimulant and 161 sec (50 frames) with KCl (to check neuronal
682 activity) or ionomycin (F_{max}). After background, fluorescence were calibrated to
683 [Ca²⁺]_i as [Ca²⁺]_i = 389 (F-F_{min})/(F_{max}-F)_nM. F_{min} was recorded by chelating Ca²⁺
684 with 10mM BAPTA (Sigma) in independent experiments and F_{max} was recorded by
685 10mM ionomycin in the presence of 10mM CaCl₂ in each experiment.

686 **Luciferase Assay:** To measure synaptic ATP levels, Cortical synaptoneuroosomes were
687 first pre-warmed and then stimulated with Gp I mGluR and NMDAR specific agonists at
688 37°C under constant shaking. Fractions of the stimulated solutions were collected at
689 the time points specified before. For treatment with various drugs, the pre-warming
690 period varied depending on the pre-incubation time of the drug before the stimulants
691 were added. Collected fractions were added to an equal volume of boiling water to
692 extract the ATP as described previously (Yang et al., 2002). The lysates were then
693 used for quantification of soluble ATP molecules using luciferase-based commercial
694 ATP quantification kit (ATP Determination kit, Thermo Fisher, Cat.no. A22066) with
695 the help of a standard curve. For measuring ATP/ADP ratio from cortical neurons,

696 cells were stimulated for specified time points and lysed with lysis buffer [containing
697 in mM: 50 Tris-Cl (pH-7.4), 150 NaCl, 5 MgCl₂, 1% Triton-X-100, supplemented with
698 EDTA free protease inhibitor complex (Sigma, cat. no. S8830) and phosphatase
699 inhibitor cocktail (Roche, ref.no. 04906837001)]. Lysates were then centrifuged at
700 20,000g for 20 minutes and supernatants were used for measuring ATP using
701 luciferase-based protocol. This was followed by a step converting ADP to ATP which
702 was then used to measure the ATP and ADP level together constituting the bulk of the
703 adenine nucleotides. This was done using a commercially available luminescence-
704 based kit (ADP/ATP ratio kit, Abcam, cat.no. ab65313) following the user manual
705 suggested by the manufacturer.

706 **Image Analysis:** Image analysis was done using Fiji (ImageJ based image processing
707 package) and IMARIS 9.0 (Bitplane, Oxford instrument company, Belfast, UK)
708 software. For fluorescence intensity quantification, confocal stacks were collapsed
709 using the sum slice projection method and mean intensity was quantified from the
710 cells. MAP2B positive cells were used for the identification of neurons and quantified
711 mean intensity values were used for normalization. For quantifying colocalization,
712 Pearson's correlation coefficient (PCC) was measured for the cell body and proximal
713 dendrite region (<50 μ m). For the coefficient analysis, the measurement was done
714 after manual thresholding with a threshold value of 155 for a 12bit image format. For
715 time frame analysis, mean fluorescence intensity was quantified for the imaged
716 dendritic region from each time frame. Time frame analysis was done using the time
717 series analyzer V3 plug-in from Fiji. Representative images for ratiometric

718 quantifications were generated using the Ratio Plus plug from Fiji where the image
719 was generated by calculating pixel by pixel intensity ratio between two channels.

720 **Statistical Analysis:** Statistical comparisons were done using GraphPad Prism (Prism
721 7.01, GraphPad Software Inc, La Jolla, CA, USA). For group comparisons, the data
722 distributions were first tested for normality using the Kolmogorov-Smirnov Goodness-
723 of-Fit Test or Shapiro-Wilk normality test. Depending on the distribution, either
724 parametric or non-parametric tests were used to quantify statistical significance. For
725 groups with <4 data points, the inherent distribution was considered to follow
726 Gaussian distribution unless mentioned. For comparing two groups, Student's t-test
727 (two-tailed, paired/unpaired) was done to calculate statistical significance. Multiple
728 group comparisons were made using one-way ANOVA followed by Bonferroni's
729 multiple comparison test for parametric distribution and Kruskal-Wallis's test
730 followed by Dunn's multiple comparison test. Two-way ANOVA followed by Holm
731 Sidak's multiple comparison test was performed for comparing multiple groups at
732 various time points. For calculating the variance of the basal ATP/(ATP+ADP) ratio,
733 values obtained from different plates from multiple cell culture experiments were
734 considered. For calculating the variance of basal synaptic ATP level at 0 min,
735 synaptoneurosomal ATP content quantified from multiple animals were considered.
736 For calculating the variance of ATP/ADP ratio at 0 min in live imaging experiments,
737 values obtained from neurons from multiple culture experiments were considered. For
738 calculating the basal fluorescence intensity variance in the immunolabelling and
739 FUNCAT experiments, intensity values obtained from different cells obtained from
740 multiple culture experiments were considered. For calculating the phospho/total

741 ratio of a protein, the phospho form, and the total protein was probed in individual
742 blots and normalized to their corresponding tubulin levels for every time point.
743 Further, a ratio of the two normalized values (i.e. normalized phospho/normalized
744 total) was considered as the phospho/total ratio. The ratio for all the time points are
745 expressed as a fraction of the initial 0 min value. Data are presented as mean \pm SEM
746 in the case of bar graphs. Data presented in box plots show the distribution of all data
747 points for the group including minimum and maximum values. The box extends from
748 25th to 75th percentile with the middlemost line representing the median of the
749 dataset. Whiskers range from minimum to maximum data point. * $p < 0.05$ was
750 considered statistically significant.

751 **Acknowledgment**

752 We are thankful to the Central Imaging and Flow-cytometry Facility (CIFF), NCBS for
753 allowing us to use the LSM 780 and FV3000 confocal microscopes, NCBS animal house
754 facility for generously maintaining the rat colony needed for experimentation. We
755 extend our gratitude to Professor M.K. Mathew and Dr. Tina Mukherjee for their
756 helpful comments and discussions. We thank Chaitra Ananda, Amirthavarshini
757 Devarajan, and Sonu P. Kurian for their gracious efforts in experimental support and
758 data analysis. The work was funded by the NeuroStem grant
759 (BT/IN/Denmark/07/RSM/2015-2016), Center for Brain Development and Repair
760 (CBDR) (BT/MB-CNDS/2013) and the Department of Biotechnology, Govt. of India. We
761 thank Dr. Garry Yellen, Harvard University for his useful suggestions on PercevalHR
762 experiments.

763

764

Author contribution

765 SGD designed and performed the experiments, analyzed data and co-wrote the
766 manuscript, SDS performed Ephys experiments and analyzed data, SCB performed
767 Calcium imaging experiments and analyzed data, SC provided resources, AB provided
768 resources, analyzed data and co-wrote the manuscript, RM conceptualized the
769 question, designed experiments, provided resources, and co-wrote the manuscript.

770

Conflict of Interest

771 The authors declare that they have no conflict of interests.

772

References:

- 773 1. Mink JW, Blumenschine RJ, Adams DB. Ratio of central nervous system to body
774 metabolism in vertebrates: its constancy and functional basis. *Am J Physiol*
775 *Integr Comp Physiol*. 1981;241(3):R203-12.
- 776 2. Fox PT, Raichle ME. Focal physiological uncoupling of cerebral blood flow and
777 oxidative metabolism during somatosensory stimulation in human subjects. *Proc*
778 *Natl Acad Sci U S A*. 1986;83(4):1140-4.
- 779 3. Fox PT, Mintun MA, Reiman EM, Raichle ME. Enhanced detection of focal brain
780 responses using intersubject averaging and change-distribution analysis of
781 subtracted PET images. *J Cereb Blood Flow Metab*. 1988;8(5):642-53.
- 782 4. Attwell D, Laughlin SB. An energy budget for signaling in the grey matter of the
783 brain. *J Cereb Blood Flow Metab*. 2001;21(10):1133-45.
- 784 5. Harris JJ, Jolivet R, Attwell D. Synaptic energy use and supply. *Neuron*.

- 785 2012;75(5):762-77.
- 786 6. Gafaniz R, Sanches JM. ATP consumption and neural electrical activity: a
787 physiological model for brain imaging. *2010 Annu Int Conf IEEE Eng Med Biol Soc*
788 *EMBC'10*. 2010;5480-3.
- 789 7. Zhu F, Wang R, Pan X, Zhu Z. Energy expenditure computation of a single
790 bursting neuron. *Cogn Neurodyn*. 2019;13(1):75-87.
- 791 8. Misgeld T, Schwarz TL. Mitostasis in neurons: maintaining mitochondria in an
792 extended cellular architecture. *Neuron*. 2017;96(3):651-66.
- 793 9. Rangaraju V, Calloway N, Ryan TA. Activity-driven local ATP synthesis is
794 required for synaptic function. *Cell*. 2014;156(4):825-35.
- 795 10. Pathak D, Shields LY, Mendelsohn BA, Haddad D, Lin W, Gerencser AA, Kim H,
796 Brand MD, Edwards RH, Nakamura K. The role of mitochondrially derived ATP in
797 synaptic vesicle recycling. *J Biol Chem*. 2015;290(37):22325-36.
- 798 11. Hsu WL, Chung HW, Wu CY, Wu HI, Lee YT, Chen EC, Fang W, Chang YC.
799 Glutamate stimulates local protein synthesis in the axons of rat cortical neurons
800 by activating α -amino-3-hydroxy-5-methyl-4-isoxazolepropionic acid (AMPA)
801 receptors and metabotropic glutamate receptors. *J Biol Chem*.
802 2015;290(34):20748-60.
- 803 12. Kos A, Wanke KA, Gioio A, Martens GJ, Kaplan BB, Aschrafi A. Monitoring mrna
804 translation in neuronal processes using fluorescent non-canonical amino acid
805 tagging. *J Histochem Cytochem*. 2016;64(5):323-33.

- 806 13. Rangaraju V, Lauterbach M, Schuman EM. Spatially stable mitochondrial
807 compartments fuel local translation during plasticity. *Cell*. 2019;176(1-2):73-
808 84.e15.
- 809 14. Rangaraju V, tom Dieck S, Schuman EM. Local translation in neuronal
810 compartments: how local is local? *EMBO Rep*. 2017;18(5):693-711.
- 811 15. Mery F, Kawecki TJ. A cost of long-term memory in drosophila. *Science (80-)*.
812 2005;308(5725):1148.
- 813 16. Plaçais PY, Preat T. To favor survival under food shortage, the brain disables
814 costly memory. *Science (80-)*. 2013;339(6118):440-2.
- 815 17. Abraham WC, Williams JM. LTP maintenance and its protein synthesis-
816 dependence. *Neurobiol Learn Mem*. 2008;89(3):260-8.
- 817 18. Schwanhüusser B, Busse D, Li N, Dittmar G, Schuchhardt J, Wolf J, Chen W,
818 Selbach M. Global quantification of mammalian gene expression control.
819 *Nature*. 2011;473(7347):337-42.
- 820 19. Huber KM, Kayser MS, Bear MF. Role for rapid dendritic protein synthesis in
821 hippocampal depression. *Science (80-)*. 2000;288(May):1254-6.
- 822 20. Luchelli L, Thomas MG, Boccaccio GL. Synaptic control of mRNA translation by
823 reversible assembly of Xrn1 bodies. *J Cell Sci*. 2015;128(8):1542-54.
- 824 21. Scheetz AJ, Nairn AC, Constantine-paton M. NMDA receptor-mediated control of
825 protein synthesis at developing synapses. *Nat Neurosci*. 2000;211-6.
- 826 22. Hunt DL, Castillo PE. **Synaptic plasticity of NMDA receptors: mechanisms and**

- 827 **functional implications.** *Curr Opin Neurobiol.* 2012;22(3):496-508.
- 828 23. Malenka L. NMDA receptor-dependent long-term potentiation and long-term
829 depression (LTP/LTD). *Cold Spring Harb Perspect Biol.* 2012;1-16.
- 830 24. Bear MF, Huber KM, Warren ST. The mGluR theory of fragile x mental
831 retardation. *Trends Neurosci.* 2004;27(7):370-7.
- 832 25. Marinangeli C, Didier S, Ahmed T, Caillerez R, Domise M, Laloux C, Bégard S,
833 Carrier S, Colin M, Marchetti P, et al. AMP-activated protein kinase is essential
834 for the maintenance of energy levels during synaptic activation. *IScience.*
835 2018;9:1-13.
- 836 26. Manlio Díaz-García C, Mongeon R, Lahmann C, Koveal D, Zucker H,
837 Correspondence GY, Yellen G. Neuronal stimulation triggers neuronal glycolysis
838 and not lactate uptake cell metabolism article neuronal stimulation triggers
839 neuronal glycolysis and not lactate uptake. *Cell Metab.* 2017;26:361-374.e4.
- 840 27. Bélanger M, Allaman I, Magistretti PJ. Brain energy metabolism: focus on
841 astrocyte-neuron metabolic cooperation. *Cell Metab.* 2011;14(6):724-38.
- 842 28. Burkewitz K, Zhang Y, Mair WB. AMPK at the nexus of energetics and aging. *Cell*
843 *Metab.* 2014;20(1):10-25.
- 844 29. Potter WB, O’Riordan KJ, Barnett D, Osting SMK, Wagoner M, Burger C, Roopra
845 A. Metabolic regulation of neuronal plasticity by the energy sensor AMPK. *PLoS*
846 *One.* 2010;5(2).
- 847 30. Kong D, Dagon Y, Campbell JN, Guo Y, Yang Z, Yi X, Aryal P, Wellenstein K,

- 848 Kahn BB, Sabatini BL, et al. A postsynaptic AMPK→p21-activated kinase pathway
849 drives fasting-induced synaptic plasticity in AgRP neurons. *Neuron*.
850 2016;91(1):25-33.
- 851 31. Sutton MA, Wall NR, Aakalu GN, Schuman EM. Regulation of dendritic protein
852 synthesis by miniature synaptic events. *Science* (80-). 2004;304(5679):1979-83.
- 853 32. Fishbein I, Segal M. Miniature synaptic currents become neurotoxic to
854 chronically silenced neurons. *Cereb Cortex*. 2007;17(6):1292-306.
- 855 33. Zhu G, Du L, Jin L, Offenhäusser A. Effects of morphology constraint on
856 electrophysiological properties of cortical neurons. *Sci Rep*. 2016;6(February):1-
857 10.
- 858 34. Dichter MA. Rat cortical neurons in cell culture: culture methods, cell
859 morphology, electrophysiology, and synapse formation. *Brain Res*.
860 1978;149(2):279-93.
- 861 35. Neumann JR, Dash-Wagh S, Jack A, Räk A, Jüngling K, Hamad MIK, Pape HC,
862 Kreutz MR, Puskarjov M, Wahle P. The primate-specific peptide Y-p30 regulates
863 morphological maturation of neocortical dendritic spines. *PLoS One*.
864 2019;14(2):1-23.
- 865 36. Dichter MA, Lisak J, Biales B. Action potential mechanism of mammalian
866 cortical neurons in cell culture. *Brain Res*. 1983;289(1-2):99-107.
- 867 37. Charlesworth P, Cotterill E, Morton A, Grant SGN, Eglén SJ. Quantitative
868 differences in developmental profiles of spontaneous activity in cortical and

- 869 hippocampal cultures. *Neural Dev.* 2015;10(1):1-10.
- 870 38. Kute PM, Ramakrishna S, Neelagandan N, Chattarji S, Muddashetty RS. NMDAR
871 mediated translation at the synapse is regulated by MOV10 and FMRP. *Mol*
872 *Brain.* 2019;12(1):1-14.
- 873 39. Cottrell JR, Dubé GR, Egles C, Liu G. Distribution, density, and clustering of
874 functional glutamate receptors before and after synaptogenesis in hippocampal
875 neurons. *J Neurophysiol.* 2000;84(3):1573-87.
- 876 40. Tantama M, Martínez-François JR, Mongeon R, Yellen G. Imaging energy status
877 in live cells with a fluorescent biosensor of the intracellular ATP-to-ADP ratio.
878 *Nat Commun.* 2013;4(May).
- 879 41. Pedersen SF, Jørgensen NK, Damgaard I, Schousboe A, Hoffmann EK.
880 Mechanisms of $\text{pH}_{(i)}$ regulation studied in individual neurons cultured from
881 mouse cerebral cortex. *J Neurosci Res.* 1998;51(4):431-41.
- 882 42. Biffi E, Regalia G, Menegon A, Ferrigno G, Pedrocchi A. The influence of
883 neuronal density and maturation on network activity of hippocampal cell
884 cultures: a methodological study. *PLoS One.* 2013;8(12).
- 885 43. Ivenshitz M, Segal M. Neuronal density determines network connectivity and
886 spontaneous activity in cultured hippocampus. *J Neurophysiol.*
887 2010;104(2):1052-60.
- 888 44. Mangan PS, Kapur J. Factors underlying bursting behavior in a network of
889 cultured hippocampal neurons exposed to zero magnesium. *J Neurophysiol.*

- 890 2004;91(2):946-57.
- 891 45. Vergara RC, Jaramillo-Riveri S, Luarte A, Moënné-Loccoz C, Fuentes R, Couve A,
892 Maldonado PE. The energy homeostasis principle: neuronal energy regulation
893 drives local network dynamics generating behavior. *Front Comput Neurosci*.
894 2019;13(July):1-18.
- 895 46. Dieterich DC, Hodas JJJ, Gouzer G, Shadrin IY, Ngo JT, Triller A, Tirrell DA,
896 Schuman EM. In situ visualization and dynamics of newly synthesized proteins in
897 rat hippocampal neurons. *Nat Neurosci*. 2010;13(7):897-905.
- 898 47. Ferrara NC, Jarome TJ, Cullen PK, Orsi SA, Kwapis JL, Trask S, Pullins SE,
899 Helmstetter FJ. GluR2 endocytosis-dependent protein degradation in the
900 amygdala mediates memory updating. *Sci Rep*. 2019;9(1):1-10.
- 901 48. Sheehan P, Zhu M, Beskow A, Vollmer C, Waites CL. Activity-dependent
902 degradation of synaptic vesicle proteins requires Rab35 and the ESCRT pathway.
903 *J Neurosci*. 2016;36(33):8668-86.
- 904 49. Jarome TJ, Werner CT, Kwapis JL, Helmstetter FJ. Activity dependent protein
905 degradation is critical for the formation and stability of fear memory in the
906 amygdala. *PLoS One*. 2011;6(9).
- 907 50. Richter JD, Collier J. Pausing on polyribosomes: make way for elongation in
908 translational control. *Cell*. 2015;163(2):292-300.
- 909 51. Maus M, Torrens Y, Gauchy C, Bretin S, Nairn AC, Glowinski J, Premont J. 2-
910 deoxyglucose and NMDA inhibit protein synthesis in neurons and regulate

- 911 phosphorylation of elongation factor-2 by distinct mechanisms. *J Neurochem.*
912 2006;96(3):815-24.
- 913 52. Ryazanov Alexey G., Shestakova Elena A. NPG. Phosphorylation of elongation
914 factor 2 by EF2-kinase affects the rate of translation. *Nature.* 1988;334(14):170-
915 3.
- 916 53. Nairn AC, Bhagat B, Palfrey HC. Identification of calmodulin-dependent protein
917 kinase iii and its major m(r) 100,000 substrate in mammalian tissues. *Proc Natl*
918 *Acad Sci U S A.* 1985;82(23):7939-43.
- 919 54. Richter JD. RNA and the synapse. *Rna.* 2015;21(4):716-7.
- 920 55. Ryazanov AG, Davydova EK. Mechanism of elongation factor 2 (EF-2) inactivation
921 upon phosphorylation: phosphorylated EF-2 is unable to catalyze translocation.
922 *FEBS Lett.* 1989;251(1-2):187-90.
- 923 56. Takei N, Kawamura M, Ishizuka Y, Kakiya N, Inamura N, Namba H, Nawa H.
924 Brain-derived neurotrophic factor enhances the basal rate of protein synthesis
925 by increasing active eukaryotic elongation factor 2 levels and promoting
926 translation elongation in cortical neurons. *J Biol Chem.* 2009;284(39):26340-8.
- 927 57. Browne GJ, Finn SG, Proud CG. Stimulation of the AMP-activated protein kinase
928 leads to activation of eukaryotic elongation factor 2 kinase and to its
929 phosphorylation at a novel site, serine 398. *J Biol Chem.* 2004;279(13):12220-
930 31.
- 931 58. Hawley SA, Davison M, Woods A, Davies SP, Beri RK, Carling D, Hardie DG.

- 932 Characterization of the AMP-activated protein kinase kinase from rat liver and
933 identification of threonine 172 as the major site at which it phosphorylates
934 AMP-activated protein kinase. *J Biol Chem.* 1996;271(44):27879-87.
- 935 59. Joseph BK, Liu HY, Francisco J, Pandya D, Donigan M, Gallo-Ebert C, Giordano
936 C, Bata A, Nickels JT. Inhibition of AMP kinase by the protein phosphatase 2a
937 heterotrimer, pp2appp2r2d. *J Biol Chem.* 2015;290(17):10588-98.
- 938 60. Voss M, Paterson J, Kellsall IR, Martín-Granados C, Hastie CJ, Peggie MW, Cohen
939 PTW. Ppm1E is an in cellulo AMP-activated protein kinase phosphatase. *Cell*
940 *Signal.* 2011;23(1):114-24.
- 941 61. Wang L, Brautigan DL. α -snap inhibits AMPK signaling to reduce mitochondrial
942 biogenesis and dephosphorylates Thr¹⁷² in AMPK α in vitro. *Nat Commun.*
943 2013;4:1559.
- 944 62. Woods A, Dickerson K, Heath R, Hong SP, Momcilovic M, Johnstone SR, Carlson
945 M, Carling D. Ca²⁺/calmodulin-dependent protein kinase kinase- β acts upstream
946 of AMP-activated protein kinase in mammalian cells. *Cell Metab.* 2005;2(1):21-
947 33.
- 948 63. Maus M, Marin P, Israël M, Glowinski J, Prémont J. Pyruvate and lactate protect
949 striatal neurons against n-methyl-d-aspartate-induced neurotoxicity. *Eur J*
950 *Neurosci.* 1999;11(9):3215-24.
- 951 64. Kim J, Yang G, Kim Y, Kim J, Ha J. AMPK activators: mechanisms of action and
952 physiological activities. *Exp Mol Med.* 2016;48(4):1-12.

- 953 65. Yoon Byung C., Zivraj Krishna H, Holt CE. Local translation and mRNA trafficking
954 in axon pathfinding. *Results Probl Cell Differ* 2009;48:269-88.
- 955 66. Spillane M, Ketschek A, Merianda TT, Twiss JL, Gallo G. Mitochondria coordinate
956 sites of axon branching through localized intra-axonal protein synthesis. *Cell*
957 *Rep.* 2013;5(6):1564-75.
- 958 67. Hovy Ho-Wai Wong A, Qiaojin Lin J, Strö hl F, Harris WA, Kaminski CF, Holt CE,
959 Ho-Wai Wong H, udio Gouveia Roque C, Cioni J-M, Cagnetta R, et al. RNA
960 docking and local translation regulate site-specific axon remodeling in vivo
961 article RNA docking and local translation regulate site-specific axon remodeling
962 in vivo. *Neuron.* 2017;95:852-68.
- 963 68. Cajigas J, Will T, Schuman EM. Protein homeostasis and synaptic plasticity.
964 2010;29(16):2746-52.
- 965 69. Rosenberg T, Gal-ben-ari S, Dieterich DC, Kreutz MR, Ziv NE. The roles of
966 protein expression in synaptic plasticity and memory consolidation.
967 2014;7(November):1-14.
- 968 70. Nödling AR, Spear LA, Williams TL, Luk LYP, Tsai YH. Using genetically
969 incorporated unnatural amino acids to control protein functions in mammalian
970 cells. *Essays Biochem.* 2019;63(2):237-66.
- 971 71. Alvarez-Castelao B, Schuman EM. The regulation of synaptic protein turnover. *J*
972 *Biol Chem.* 2015;290(48):28623-30.
- 973 72. Weiler IJ, Spangler CC, Klintsova AY, Grossman AW, Kim SH, Bertaina-Anglade V,

- 974 Khaliq H, de Vries FE, Lambers F a E, Hatia F, et al. Fragile x mental retardation
975 protein is necessary for neurotransmitter-activated protein translation at
976 synapses. *Proc Natl Acad Sci USA*. 2004;101(50):17504-9.
- 977 73. Bellone C, Lüscher C, Mameli M. Mechanisms of synaptic depression triggered by
978 metabotropic glutamate receptors. *Cell Mol Life Sci*. 2008;65(18):2913-23.
- 979 74. Schulte G. The class frizzled receptors. *Pharmacol Rev*. 2010;62(4):632-67.
- 980 75. Jörntell H, Hansel C. Synaptic memories upside down: bidirectional plasticity at
981 cerebellar parallel fiber-purkinje cell synapses. *Neuron*. 2006;52(2):227-38.
- 982 76. Yuan Y, Huo H, Fang T. Effects of metabolic energy on synaptic transmission and
983 dendritic integration in pyramidal neurons. *Front Comput Neurosci*.
984 2018;12(September):1-13.
- 985 77. Peth A, Nathan JA, Goldberg AL. The ATP costs and time required to degrade
986 ubiquitinated proteins by the 26s proteasome. *J Biol Chem*. 2013;288(40):29215-
987 22.
- 988 78. Ashrafi G, Wu Z, Farrell RJ, Ryan TA. GLUT4 mobilization supports energetic
989 demands of active synapses. *Neuron*. 2017;93(3):606-615.e3.
- 990 79. Johanns M, Pyrdit Ruys S, Houddane A, Vertommen D, Herinckx G, Hue L, Proud
991 CG, Rider MH. Direct and indirect activation of eukaryotic elongation factor 2
992 kinase by AMP-activated protein kinase. *Cell Signal*. 2017;36(April):212-21.
- 993 80. Narayanan U, Nalavadi V, Nakamoto M, Pallas DC, Ceman S, Bassell GJ, Warren
994 ST. FMRP phosphorylation reveals an immediate-early signaling pathway

- 995 triggered by group i mGluR and mediated by PP2a. *J Neurosci.*
996 2007;27(52):14349-57.
- 997 81. Hollingsworth EB, McNeal ET, Burton JL, Williams RJ, Daly JW, Creveling CR.
998 Biochemical characterization of a filtered synaptoneurosome preparation from
999 guinea pig cerebral cortex: cyclic adenosine 3':5'-monophosphate-generating
1000 systems, receptors, and enzymes. *J Neurosci.* 1985;5(8):2240-53.
- 1001 82. Nalavadi VC, Muddashetty RS, Gross C, Bassell GJ. Dephosphorylation-induced
1002 ubiquitination and degradation of FMRP in dendrites: a role in immediate early
1003 mGluR-stimulated translation. *J Neurosci.* 2012;32(8):2582-7.
- 1004 83. Yang NC, Ho WM, Chen YH, Hu ML. A convenient one-step extraction of cellular
1005 ATP using boiling water for the luciferin-luciferase assay of atp. *Anal Biochem.*
1006 2002;306(2):323-7.
- 1007 84. Banker G, Goslin K. Culturing nerve cells. In: Cellular and molecular
1008 neuroscience series. 1998. p. 666.
- 1009 85. Bilican B, Livesey MR, Haghi G, Qiu J, Burr K, Siller R, Hardingham GE, Wyllie
1010 DJA, Chandran S. Physiological normoxia and absence of EGF is required for the
1011 long-term propagation of anterior neural precursors from human pluripotent
1012 cells. *PLoS One.* 2014;9(1).
- 1013 86. Livesey MR, Bilican B, Qiu J, Rzechorzek NM, Haghi G, Burr K, Hardingham GE,
1014 Chandran S, Wyllie DJA. Maturation of AMPAR composition and the gabaar
1015 reversal potential in hpsc-derived cortical neurons. *J Neurosci.*
1016 2014;34(11):4070-5.

1017 **Figure Legends:**

1018 **Figure 1**

1019 **mGluR Dependent Protein Synthesis Presents the Bulk of the Metabolic Burden**
1020 **Following Glutamate Stimulation in Cortical Neurons:**

1021 (A) Schematic depicting experimental workflow for the measurement of the
1022 ATP/ATP+ADP ratio using luciferase-based methods following glutamate
1023 stimulation in the presence or absence of various drugs from **high-density**
1024 **cultured cortical neurons at** 15 days *in-vitro* (DIV 15).

1025 (B) Bar graph representing the normalized average value of the neuronal
1026 ATP/ATP+ADP ratio on the basal condition, on glutamate stimulation for 5
1027 minutes, on glutamate stimulation with anisomycin (25 μ M) and on glutamate
1028 stimulation with cycloheximide (350 μ M). Data presented as mean \pm SEM with
1029 scattered data points. **Values in all other groups were normalized to the basal**
1030 **group for the corresponding experiment.** **p<0.01, ***p<0.001, ****p<0.0001,
1031 n=5 independent platings. One-way ANOVA followed by Bonferroni's multiple
1032 comparison test.

1033 (C) Bar graph representing the normalized average value of neuronal
1034 ATP/ATP+ADP ratio on the basal condition, on glutamate stimulation for 5
1035 minutes, on glutamate stimulation with MPEP, on glutamate stimulation with
1036 CNQX + D-AP5 and on glutamate stimulation with CNQX + D-AP5 + anisomycin.
1037 Data presented as mean \pm SEM with scattered data points. **Values in all other**
1038 **groups were normalized to the basal group for the corresponding experiment.**

1039 * $p < 0.05$, *** $p < 0.001$, $n = 4-5$ independent platings. One-way ANOVA followed by
1040 Bonferroni's multiple comparison test.

1041 **(D)** Representative current-clamp and voltage-clamp traces showing a single
1042 neuron firing spontaneous bursts of action potentials. The traces on the right
1043 shows a single representative burst at a higher temporal resolution.

1044 **(E)** Bar graph representing the burst frequency and burst duration both in the
1045 voltage and current-clamp mode. $n = 16$ neurons from ≥ 3 independent platings.
1046 Data presented as mean \pm SEM with scattered data points.

1047 **(F)** Representative voltage-clamp traces of miniature EPSCs recorded ($V_{\text{hold}} = -$
1048 70mV) from a neuron in presence of TTX.

1049 **(G)** Bar graph representing the baseline mEPSC frequency and amplitude in the
1050 current-clamp mode. $N = 11$ neurons from ≥ 3 independent platings. Data
1051 presented as mean \pm SEM with scattered data points.

1052 **(H)** Schematic depicting experimental workflow for the measurement of the
1053 synaptic ATP level using luciferase-based methods following DHPG and NMDA
1054 treatment in the presence or absence of various drugs from cortical
1055 synaptoneuroosomes obtained from Sprague Dawley rats at postnatal day 30
1056 (P30).

1057 **(I)** Immunoblots depicting levels of PSD 95, GFAP, Synapsin 1 and tubulin in the
1058 whole cortical lysate and the synaptoneurosome preparations. Quantification
1059 representing the average fold enrichments of PSD 95, Synapsin 1 and GFAP in
1060 the synaptoneurosome preparations compared to the whole cortical lysate.

1061 Data presented as mean \pm SEM with scattered data points. Data points for all
1062 the proteins were normalized to their respective whole lysate values. ** $p < 0.05$,
1063 ** $p < 0.01$, $n \geq 7$ animals for each group. One-sample t-test.

1064 (J) Bar graph representing the normalized average value of synaptic ATP level
1065 on the basal condition, on DHPG treatment for 5 minutes, on DHPG treatment
1066 with MPEP, on DHPG treatment with anisomycin and on DHPG treatment with
1067 cycloheximide (350 μ M). Data presented as mean \pm SEM with scattered data
1068 points. Values in all other groups were normalized to the basal group for the
1069 corresponding experiment. * $p < 0.05$, $n = 8$ animals. One-way ANOVA followed by
1070 Bonferroni's multiple comparison test.

1071 (K) Bar graph representing the normalized average value of the synaptic ATP
1072 level on the basal condition, on NMDA treatment for 5 minutes and on NMDA
1073 treatment with D-AP5. Data presented as mean \pm SEM with scattered data
1074 points. Values in all other groups were normalized to the basal group for the
1075 corresponding experiment. $n = 8$ independent platings.

1076 **Figure 2**

1077 **mGluR and NMDAR impact synaptic-dendritic ATP/ADP ratio with distinct Kinetics**

1078 (A) Schematic depicting the experimental workflow for the measurement of
1079 the ATP/ADP ratio using an imaging-based approach either from somatic or
1080 from dendritic compartments of cortical neurons (DIV 15) plated at low-
1081 density.

1082 (B) Representative neurons showing changes in the PercevalHR fluorescence
1083 ratio (~ATP/ADP ratio) in somatic compartments on the bath application of
1084 DHPG and NMDA. Scale bar 10 μ m.

1085 (C) Representative neurons showing changes in the PercevalHR fluorescence
1086 ratio (~ATP/ADP ratio) in dendritic compartments on the bath application of
1087 DHPG and NMDA. Scale bar 10 μ m.

1088 (D) Average traces depicting the time course of the normalized somatic
1089 ATP/ADP ratio on the basal conditions, on DHPG treatment, and on NMDA
1090 treatment. The curved arrow on the top indicates the time when the agonists
1091 were added and kept in the imaging media. Data presented as mean +/- SEM.
1092 Values in all other groups were normalized to the 0 min group for the
1093 corresponding experiment and all the data points are represented as a fraction
1094 of the initial time point. n= 5-6 cells from ≥ 3 independent platings.

1095 (E) Average traces depicting the time course of normalized dendritic ATP/ADP
1096 ratio on the basal condition, on the basal condition in the presence of
1097 anisomycin, on DHPG treatment, on NMDA treatment, on DHPG treatment in
1098 the presence of anisomycin and on NMDA treatment in the presence of
1099 anisomycin. The curved arrow on the top indicates the time when the agonists
1100 were added and kept in the imaging media. Data presented as mean +/- SEM.
1101 Values in all other groups were normalized to the 0 min group for the
1102 corresponding experiment and all the data points are represented as a fraction
1103 of the initial time point. n= 6-9 cells from ≥ 3 independent platings.

1104 (F) Schematic depicting stimulation protocol in cortical synaptoneuroosomes for
1105 quantification of the synaptic ATP level.

1106 (G) Line graph showing the average normalized synaptic ATP level at various
1107 time points after DHPG treatment until 5 minutes of recovery in the presence
1108 or absence of anisomycin. Data presented as mean +/- SEM, * $p < 0.05$, ** $p < 0.01$,
1109 **** $p < 0.0001$ for comparison with 0 minute. ## $p < 0.01$ and ##### $p < 0.0001$ for
1110 comparison between DHPG + anisomycin. Values in all other groups were
1111 normalized to the 0 min group for the corresponding experiment and all the
1112 data points are represented as a fraction of the initial time point. $n \geq 5$ animals
1113 per group. Two-way ANOVA followed by Bonferroni's multiple comparison tests.

1114 (H) Line graph showing the average normalized synaptic ATP level at various
1115 time points after NMDA treatment until 5 minutes after recovery in the
1116 presence or absence of anisomycin. Data presented as mean +/- SEM, ** $p < 0.01$
1117 for comparison with 0 minutes. Values in all other groups were normalized to
1118 the 0 min group for the corresponding experiment and all the data points are
1119 represented as a fraction of the initial time point. $n \geq 4$ animals per group.
1120 Two-way ANOVA followed by Bonferroni's multiple comparison tests.

1121 **Figure 3:**

1122 **mGluR and NMDAR alter global translation by regulating eEF2 phosphorylation with**
1123 **distinct kinetics.**

1124 (A) Schematic depicting the experimental workflow and the stimulation
1125 protocol to visualize and quantify newly synthesized proteins through

1126 metabolic labeling at various time points following DHPG or NMDA treatment in
1127 cortical neurons DIV 15 plated at low-density.

1128 **(B)** Representative images showing newly synthesized proteins on the basal
1129 condition visualized through FUNCAT metabolic labeling (pseudo-colored) in
1130 cortical neurons. MAP2B immunolabeling was used for identifying neurons and
1131 intensity was used for normalization. Scale bar 10 μ m.

1132 **(C)** Representative images showing newly synthesized proteins visualized
1133 through FUNCAT metabolic labeling (pseudo-colored) in cortical neurons at
1134 various time points following DHPG and NMDA treatment. MAP2B
1135 immunolabeling was used for identifying neurons and intensity was used for
1136 normalization. Scale bar 10 μ m.

1137 **(D)** Line graph showing the change in the average normalized FUNCAT intensity
1138 representing the quantity of newly synthesized proteins at various time points
1139 following DHPG and NMDA treatments. Data presented as mean +/- SEM. **Data**
1140 **points in all groups were normalized to the average of the basal group.**
1141 *** $p < 0.001$ $n = 21-54$ neurons per group from 3 independent platings. Two-way
1142 ANOVA followed by Bonferroni's multiple comparison test.

1143 **(E)** Representative images showing phospho-eEF2 immunolabeling (Pseudo-
1144 colored) in low-density cortical neurons on the basal condition, on DHPG
1145 treatment for 5 minutes and on NMDA treatment for 5 minutes. MAP2B
1146 immunolabeling was used for identifying neurons and intensity was used for
1147 normalization. Scale bar 10 μ m.

1148 (F) Box plot showing phospho-eEF2 normalized intensity distribution across
1149 multiple neurons on the basal condition, on DHPG treatment for 5 minutes and
1150 on NMDA treatment for 5 minutes. Data points in all groups were normalized to
1151 the average of the basal group. The box extends from 25th to 75th percentile
1152 with the middlemost line representing the median of the dataset. Whiskers
1153 range from minimum to maximum data point. * $p < 0.05$, ** $p < 0.01$, $n = 31-49$ cells
1154 per group from 3 independent platings. One-way ANOVA followed by
1155 Bonferroni's multiple comparison test.

1156 (G) Representative immunoblots describing changes in the phospho-eEF2 and
1157 total-eEF2 levels at various time points after DHPG and NMDA treatment in
1158 cortical synaptoneurosome. Note in each case phospho and total eEF2 levels
1159 were normalized individually to their respective tubulin levels for calculating
1160 the phospho/total eEF2 ratio.

1161 (H) Line graph showing the average value of the synaptic phospho/total ratio of
1162 eEF2 at various time points after DHPG and NMDA treatment until 5 minutes of
1163 recovery. Data presented as mean \pm SEM, ** $p < 0.01$. Values in all other groups
1164 were normalized to the 0 min group for the corresponding experiment and all
1165 the data points are represented as a fraction of the initial time point.
1166 *** $p < 0.001$, **** $p < 0.0001$, $n \geq 5$ animals per group. Two-way ANOVA followed by
1167 Bonferroni's multiple comparison test.

1168

1169

1170 **Figure 4:**

1171 **mGluR modulates AMPK function through a protein synthesis-dependent feedback**
1172 **mechanism:**

1173 (A) Representative images showing phospho-AMPK immunolabeling (Pseudo-
1174 colored) in low-density cortical neurons on the basal condition, on DHPG
1175 treatment for 5 minutes and on NMDA treatment for 5 minutes. MAP2B
1176 immunolabeling was used for identifying neurons and intensity was used for
1177 normalization. Scale bar 10 μ m.

1178 (B) Box plot showing the normalized phospho-AMPK intensity distribution across
1179 multiple neurons on the basal condition, on DHPG treatment for 5 minutes and
1180 on NMDA treatment for 5 minutes. Data points in all groups were normalized to
1181 the average of the basal group. The box extends from 25th to 75th percentile
1182 with the middlemost line representing the median of the dataset. Whiskers
1183 range from minimum to maximum data point. *p<0.05, **p<0.01, n=30-46 cells
1184 per group from 3 independent platings. One-way ANOVA followed by
1185 Bonferroni's multiple comparison test.

1186 (C) Representative immunoblots describing changes in the phospho-AMPK and
1187 total-AMPK levels at various time points after DHPG treatment in cortical
1188 synaptoneurosomes in the presence or absence of anisomycin. Note in each
1189 case phospho and total AMPK levels were normalized individually to their
1190 respective tubulin levels before calculating the phospho/total ratio of AMPK.

1191 (D) Line graph showing the normalized average value of the synaptic
1192 phospho/total ratio of AMPK at various time points after DHPG treatment in the
1193 presence or absence of anisomycin. Data presented as mean +/- SEM. Values in
1194 all other groups were normalized to the 0 min group for the corresponding
1195 experiment and all the data points are represented as a fraction of the initial
1196 time point. * $p < 0.05$, ** $p < 0.01$, **** $p < 0.0001$, $n = 5$ animals per group. Two-way
1197 ANOVA followed by Bonferroni's multiple comparison test.

1198 (E) Representative immunoblots depicting the changes in the α -SNAP protein
1199 levels at various time points after DHPG treatment in cortical
1200 synaptoneuroosomes in the presence or absence of anisomycin.

1201 (F) Line graph showing the normalized average value of the synaptic α -SNAP
1202 protein levels at various time points after DHPG treatment in the presence or
1203 absence of anisomycin. Data presented as mean +/- SEM. * $p < 0.05$. Values in all
1204 other groups were normalized to the 0 min group for the corresponding
1205 experiment and all the data points are represented as a fraction of the initial
1206 time point. ** $p < 0.01$, $n \geq 4$ animals per group. Two-way ANOVA followed by
1207 Bonferroni's multiple comparison test.

1208 (G) Representative images showing the α -SNAP (cyan) and AMPK (magenta)
1209 immunolabeling in low-density cortical neurons. Merge shows the colocalization
1210 of the two channels both on the basal condition and on DHPG treatment for 5
1211 minutes. Scale bar 10 μ m. Zoomed in representative images of dendrites

1212 showing the merge of both channels on the basal and DHPG treated conditions.

1213 Scale bar 5 μ m.

1214 **(H)** Box plot depicting the quantification of co-localization through Pearson's
1215 correlation coefficient between α -SNAP and AMPK in cortical neurons on the
1216 basal condition and on DHPG treatment for 5 minutes. The box extends from
1217 25th to 75th percentile with the middlemost line representing the median of the
1218 dataset. Whiskers range from minimum to maximum data point. * $p < 0.01$, $n \geq 35$
1219 cells per group from 4 independent platings. Unpaired-sample t-test.

1220 **(I)** Representative images showing the phospho-AMPK immunolabeling (Pseudo-
1221 colored) in low-density cortical neurons on the basal condition and on DHPG
1222 treatment for 5 minutes in the presence of scrambled siRNA and in the
1223 presence of α -SNAP siRNA. MAP2B immunolabeling was used for identifying
1224 neurons and intensity was used for normalization. Scale bar 10 μ m.

1225 **(J)** Box plot showing the normalized phospho-AMPK intensity distribution across
1226 multiple neurons on the basal condition in the presence of scrambled siRNA, on
1227 DHPG treatment for 5 minutes in the presence of scrambled siRNA, on the basal
1228 condition in the presence of α -SNAP siRNA, on DHPG treatment for 5 minutes in
1229 the presence of α -SNAP siRNA. **Data points in all groups were normalized to the**
1230 **average of the scrambled siRNA basal group.** The box extends from 25th to 75th
1231 percentile with the middlemost line representing the median of the dataset.
1232 Whiskers range from minimum to maximum data point. * $p < 0.05$, $n = 29-35$ cells

1233 per group from 3 independent platings. Kruskal-Wallis test followed by Dunn's
1234 multiple comparison test.

1235 **Figure 5:**

1236 **NMDAR mediated AMPK activation is extracellular Ca²⁺-dependent.**

1237 (A) Representative immunoblots describing changes in the phospho-AMPK and
1238 total-AMPK levels at various time points after NMDA treatment in cortical
1239 synaptoneurosomes in the presence or absence of extracellular Ca²⁺. Note in
1240 each case phospho and total AMPK levels were normalized individually to their
1241 respective tubulin levels before calculating the phospho/total AMPK ratio.

1242 (B) Line graph showing the normalized average value for the synaptic
1243 phospho/total ratio of AMPK at various time points after NMDA treatment until
1244 5 minutes of recovery in the presence or absence of extracellular Ca²⁺. Data
1245 presented as mean +/- SEM. Values in all other groups were normalized to the 0
1246 min group for the corresponding experiment and all the data points are
1247 represented as a fraction of the initial time point. **p<0.01, ****p<0.0001, n= 6
1248 animals per group. Two-way ANOVA followed by Bonferroni's multiple
1249 comparison test.

1250 (C) Representative images depicting intracellular Ca²⁺ levels through Fluo8
1251 fluorescence (Pseudo-colored) of a cortical neuron plated at low-density before
1252 stimulation, 15 sec (immediate) after NMDA treatment, 300 sec (delayed) after
1253 NMDA treatment and after ionomycin treatment in the presence of 10mM Ca²⁺.
1254 Scale bar 20µm.

1255 (D) Representative time trace showing the normalized change in Fluo8
1256 fluorescence on NMDA treatment in the presence or absence of extracellular
1257 Ca^{2+} and D-AP5. Values in all other groups were normalized to the unstimulated
1258 condition for the corresponding experiment and all the data points are
1259 represented as a fraction of the initial time point. Ionomycin treatment in the
1260 presence of 10mM Ca^{2+} was used to calculate fluorescence maximum for a
1261 particular cell.

1262 (E) Box plot showing the distribution of $\Delta F/F_0$ across multiple neurons on the
1263 basal condition, on NMDA treatment in the presence Ca^{2+} , on NMDA treatment
1264 in the absence of Ca^{2+} , on NMDA treatment with D-AP5 and on NMDA treatment
1265 along with MK-801. The box extends from 25th to 75th percentile with the
1266 middlemost line representing the median of the dataset. Whiskers range from
1267 minimum to maximum data point. **** $p < 0.0001$, $n \geq 30$ neurons per group from 3
1268 independent platings. One-way ANOVA followed by Bonferroni's multiple
1269 comparison test.

1270 **Figure 6:**

1271 **Perturbation of AMPK function disrupts receptor-specific translation response:**

1272 (A) Schematic depicting the experimental workflow for quantifying p-eEF2
1273 levels and FUNCAT intensity changes on DHPG and NMDA treatment in low-
1274 density cortical neurons (DIV 15).

1275 (B) Representative images showing the phospho-eEF2 immunolabeling (Pseudo-
1276 colored) and newly synthesized proteins as FUNCAT signal (pseudo-colored) in

1277 cortical neurons on the basal condition and on DHPG (50 μ M) treatment for 5
1278 minutes in the presence or absence of AICAR (1mM). MAP2B immunolabeling
1279 was used for identifying neurons and intensity was used for normalization.
1280 Scale bar 10 μ m.

1281 **(C)** Box plot showing the normalized phospho-eEF2 intensity distribution across
1282 multiple neurons on the basal condition, on DHPG treatment for 5 minutes, on
1283 AICAR treatment and on DHPG treatment with AICAR. **Data points in all groups**
1284 **were normalized to the average of the basal group.** The box extends from 25th
1285 to 75th percentile with the middlemost line representing the median of the
1286 dataset. Whiskers range from minimum to maximum data point. * $p < 0.05$,
1287 ** $p < 0.01$, **** $p < 0.0001$, $n = 17-46$ cells per group from 3 independent platings.
1288 One-way ANOVA followed by Bonferroni's multiple comparison test.

1289 **(D)** Box plot showing the FUNCAT intensity distribution across multiple neurons
1290 on the basal condition, on DHPG treatment for 5 minutes, on AICAR treatment
1291 and on DHPG treatment with AICAR. **Data points in all groups were normalized**
1292 **to the average of the basal group.** The box extends from 25th to 75th percentile
1293 with the middlemost line representing the median of the dataset. Whiskers
1294 range from minimum to maximum data point. **** $p < 0.0001$, $n = 18-57$ cells per
1295 group from 3 independent platings. Kruskal-Wallis test followed by Dunn's
1296 multiple comparison test.

1297 **(E)** Representative images showing the phospho-eEF2 immunolabeling (Pseudo-
1298 colored) and newly synthesized proteins as FUNCAT signal (Pseudo-colored) in

1299 cortical neurons on the basal condition and on NMDA treatment for 5 minutes in
1300 the presence or absence of Compound C. MAP2B immunolabeling was used for
1301 identifying neurons and intensity was used for normalization. Scale bar 10 μ m.

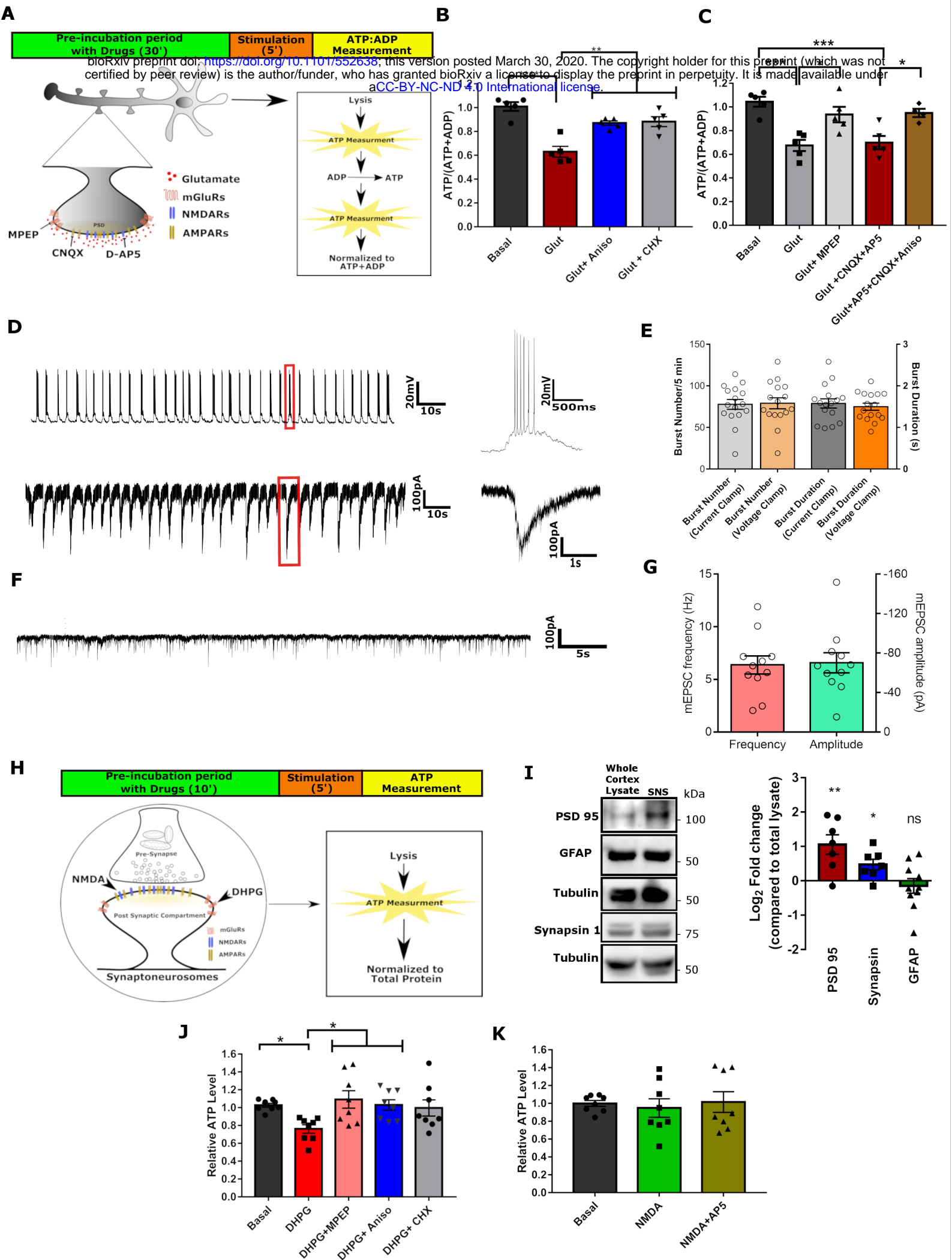
1302 **(F)** Box plot showing phospho-eEF2 intensity distribution across multiple
1303 neurons on basal condition (Vehicle control), on NMDA treatment for 5 minutes,
1304 on Compound C treatment and on NMDA treatment with Compound C. **Data**
1305 **points in all groups were normalized to the average of the basal group.** The box
1306 extends from 25th to 75th percentile with the middlemost line representing the
1307 median of the dataset. Whiskers range from minimum to maximum data point.
1308 * $p < 0.05$, ** $p < 0.01$, $n = 21-36$ cells per group from 3 independent platings.
1309 Kruskal-Wallis test followed by Dunn's multiple comparison test.

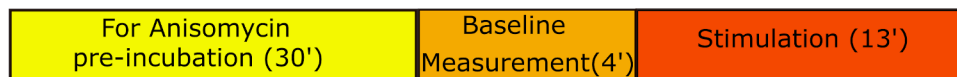
1310 **(G)** Box plot showing the FUNCAT intensity distribution across multiple neurons
1311 on the basal condition, on NMDA treatment for 5 minutes, on Compound C
1312 treatment and on NMDA treatment with Compound C. **Data points in all groups**
1313 **were normalized to the average of the basal group.** The box extends from 25th
1314 to 75th percentile with the middlemost line representing the median of the
1315 dataset. Whiskers range from minimum to maximum data point. * $p < 0.05$,
1316 ** $p < 0.01$, **** $p < 0.0001$, $n = 24-52$ cells per group from 3 independent platings.
1317 Kruskal-Wallis test followed by Dunn's multiple comparison test.

1318 **(H)** Model of the receptor-specific regulation of AMPK-eEF2 signaling axis and
1319 their subsequent effect on global translation. mGluR stimulation (Left)
1320 inactivates AMPK, a necessity for the dephosphorylation of eEF2. This, in turn,

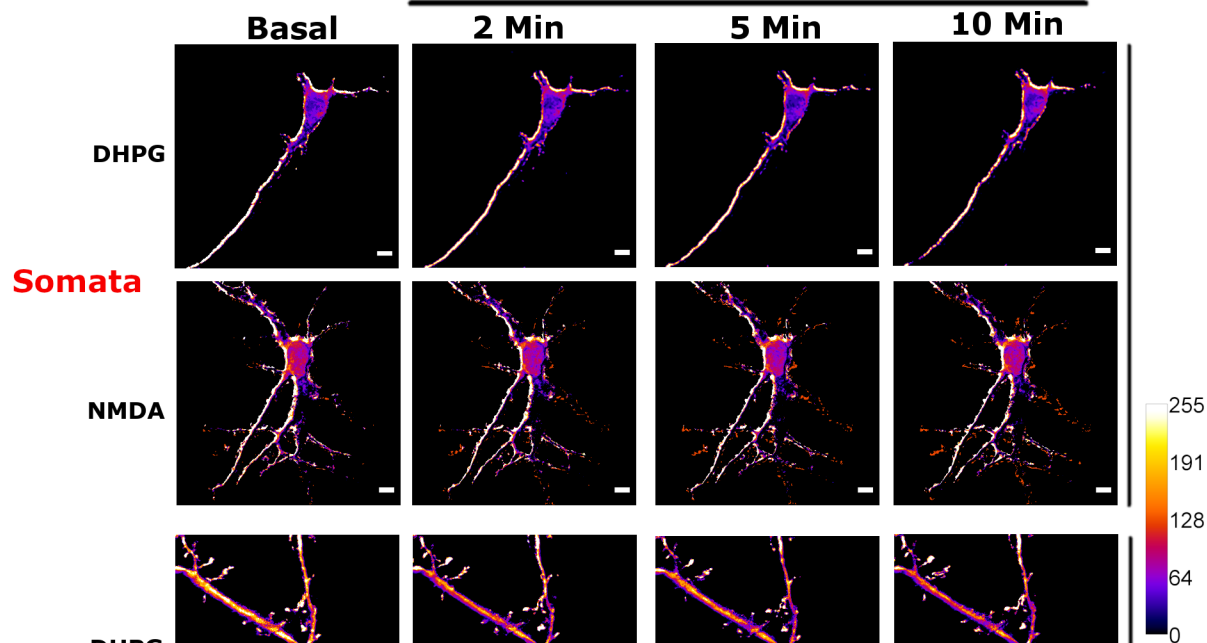
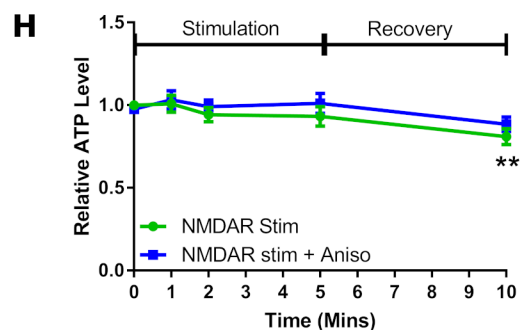
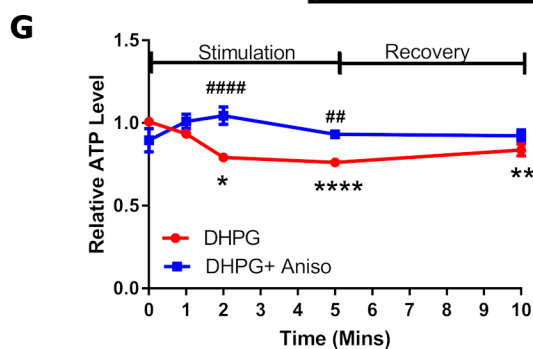
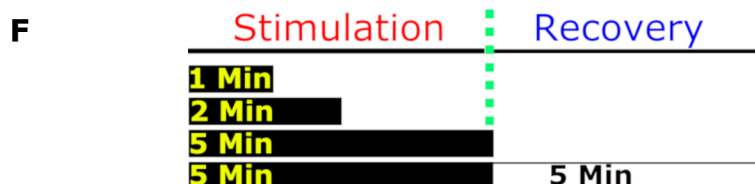
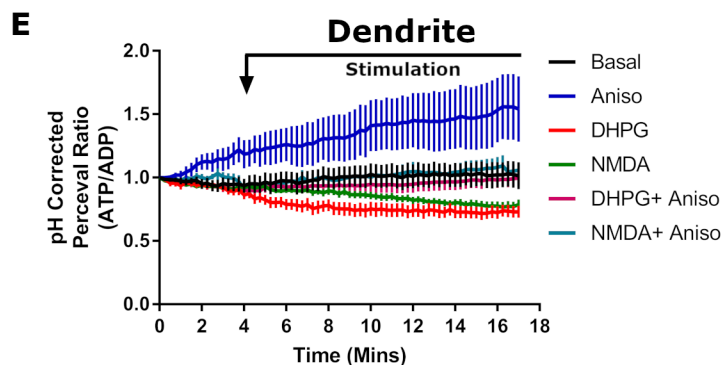
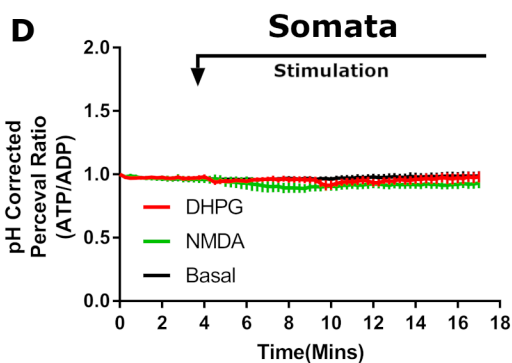
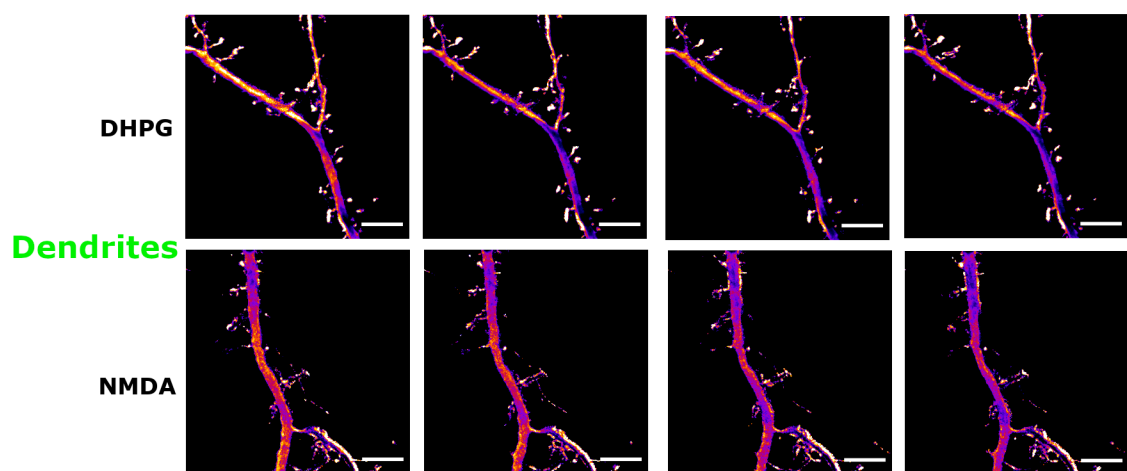
1321 leads to an enhanced protein synthesis thereby leading to the consumption of
1322 ATP. NMDAR stimulation (Right), however, led to an activation of AMPK by
1323 allowing the entry of extracellular Ca^{2+} through open NMDAR channels. This
1324 resulted in an increase in the eEF2 phosphorylation and an inhibition of global
1325 protein synthesis having no significant impact on neuronal energetics.

1326



A

bioRxiv preprint doi: <https://doi.org/10.1101/552638>; this version posted March 30, 2020. The copyright holder for this preprint (which was not certified by peer review) is the author/funder, who has granted bioRxiv a license to display the preprint in perpetuity. It is made available under aCC-BY-NC-ND 4.0 International license.

B**C**

A

Stimulation Recovery

2 Min

5 Min

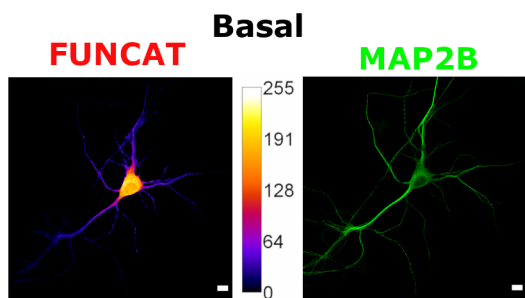
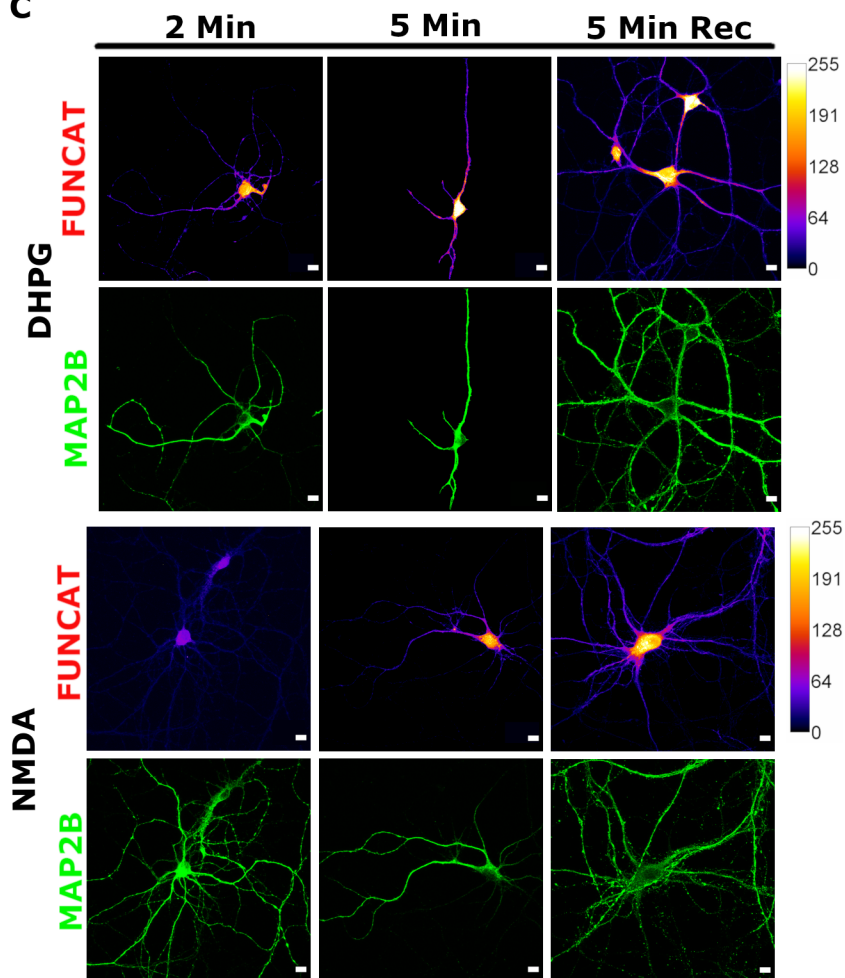
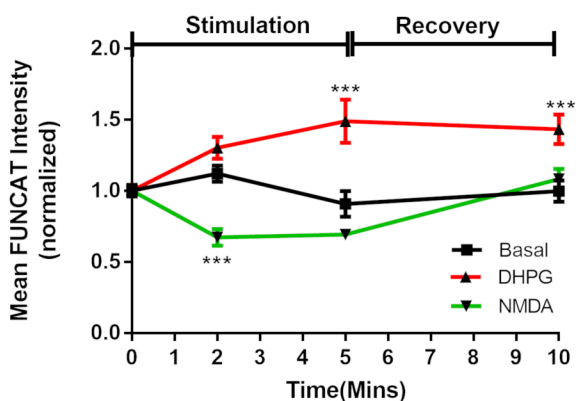
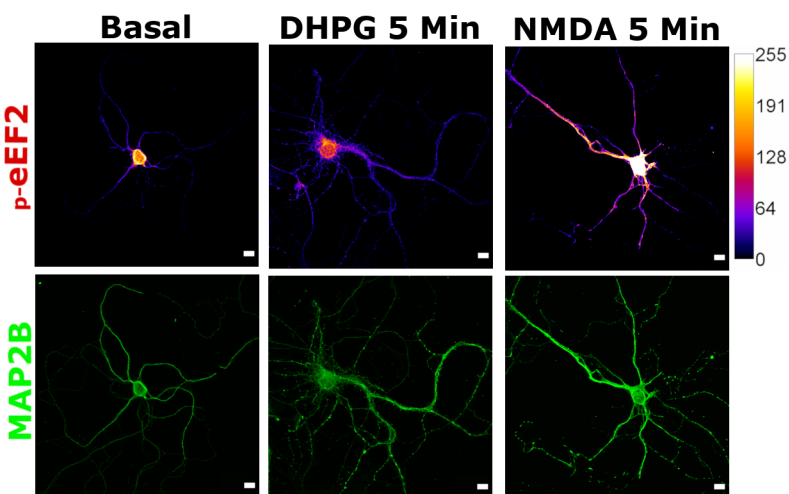
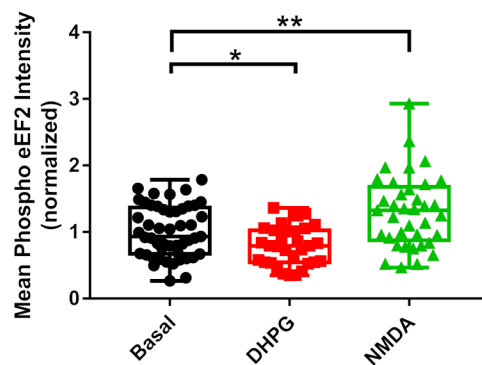
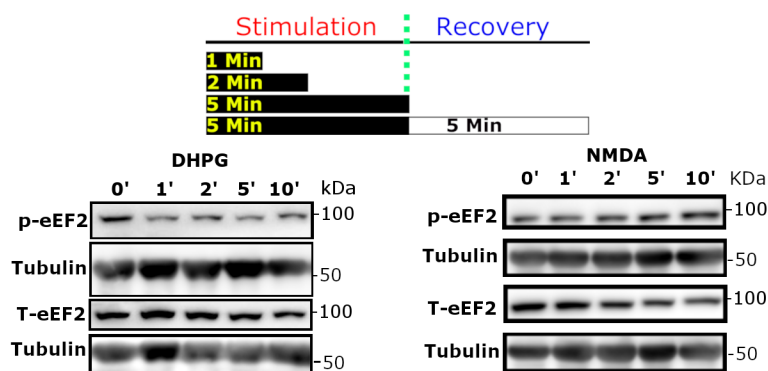
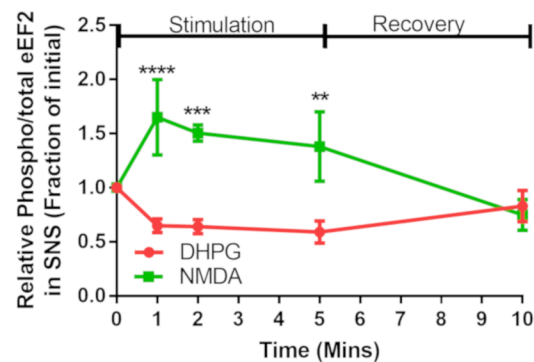
5 Min

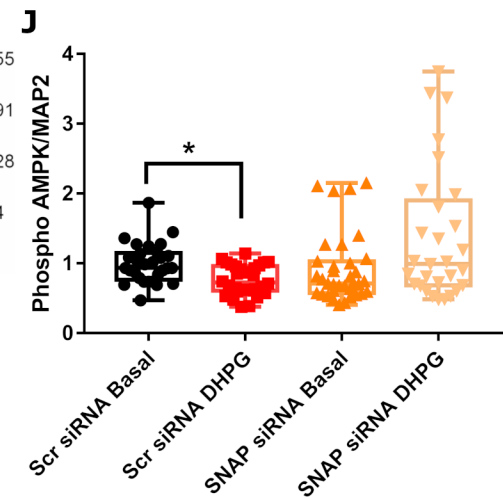
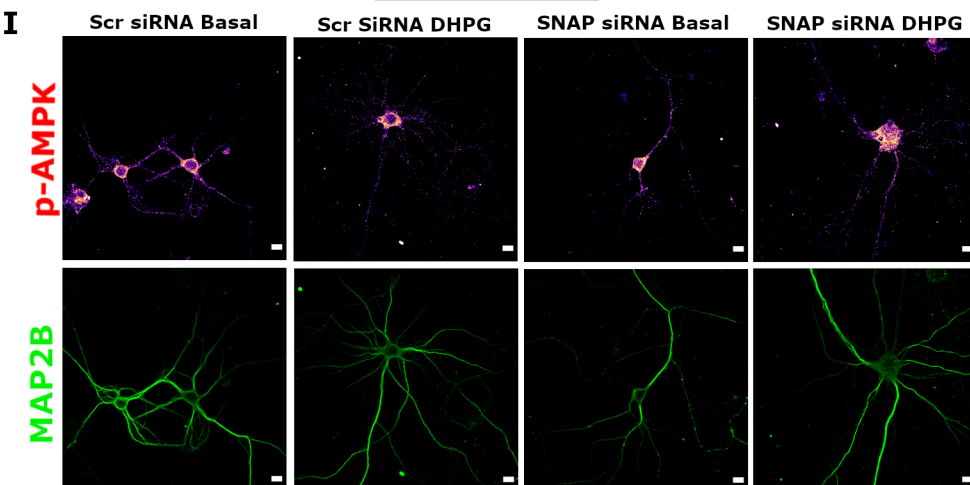
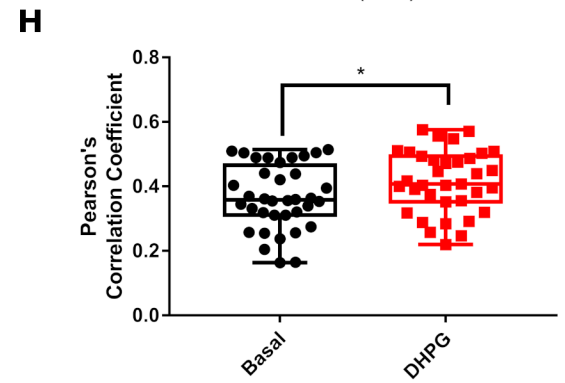
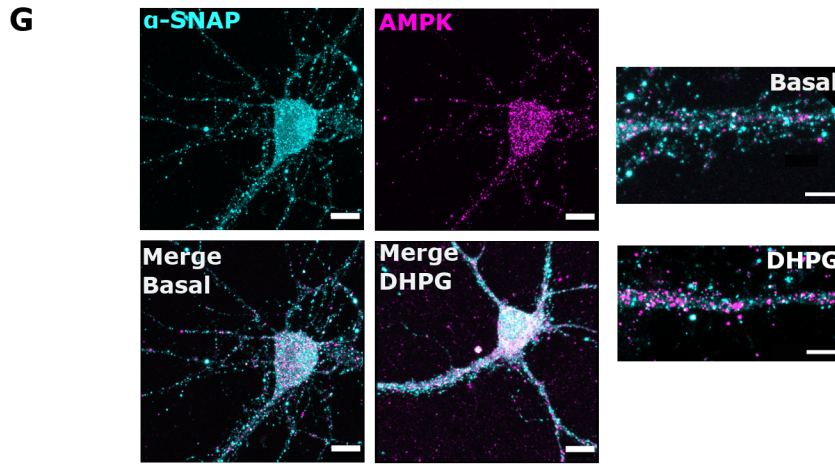
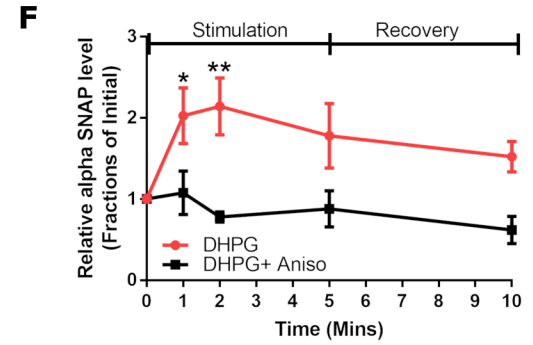
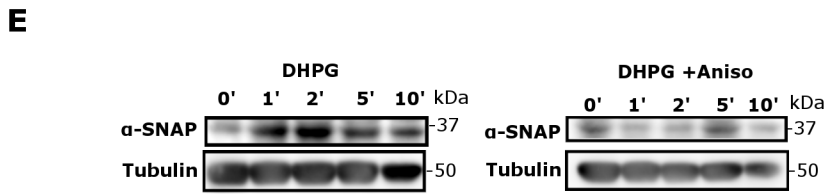
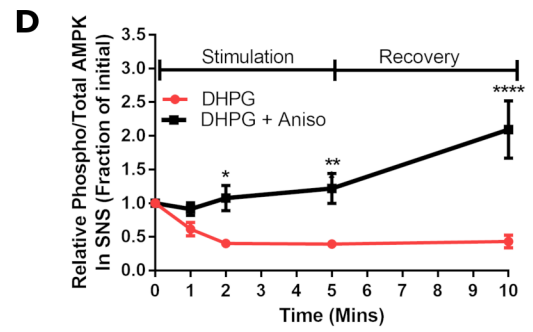
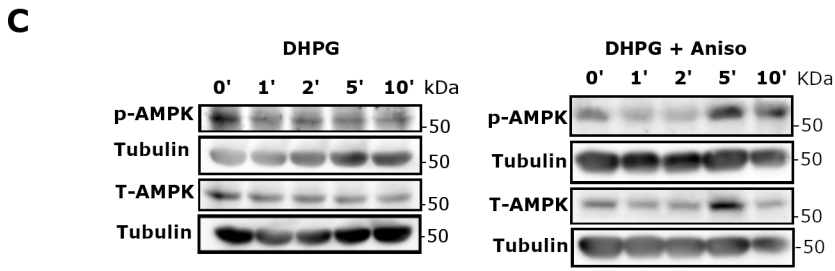
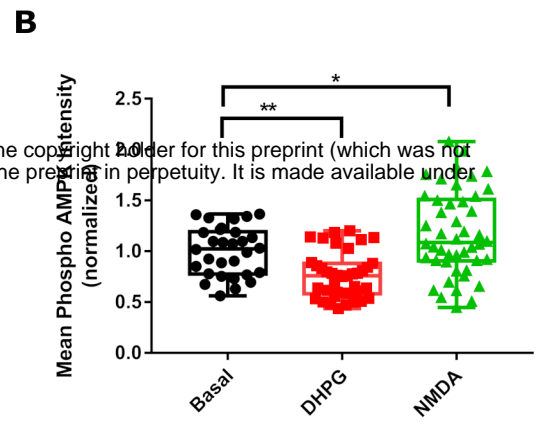
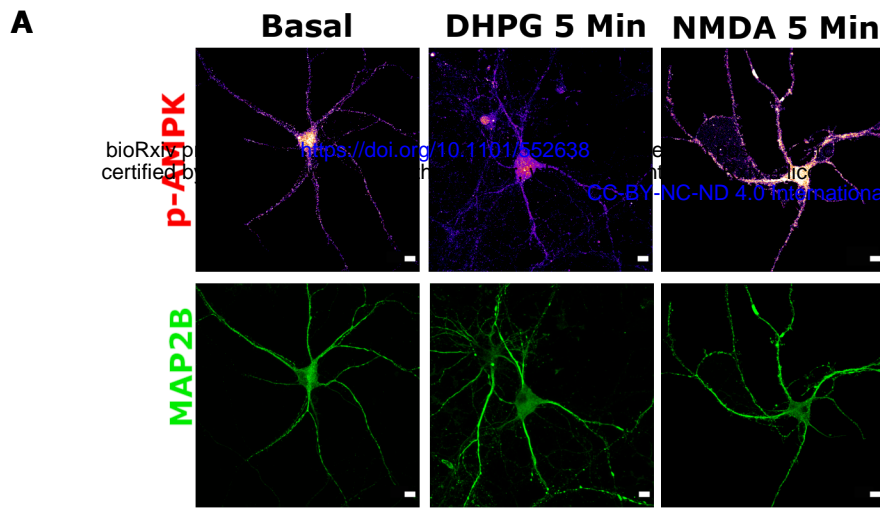
5 Min

1 Hr in Met free DMEM

1 Hr DMEM + AHA Incubation

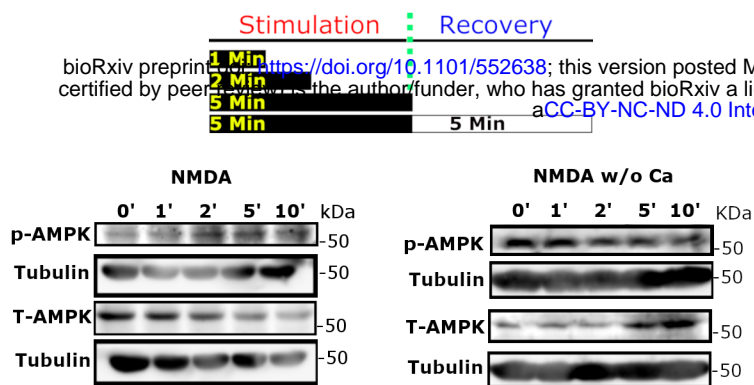
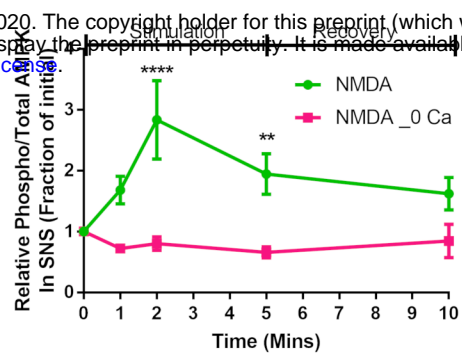
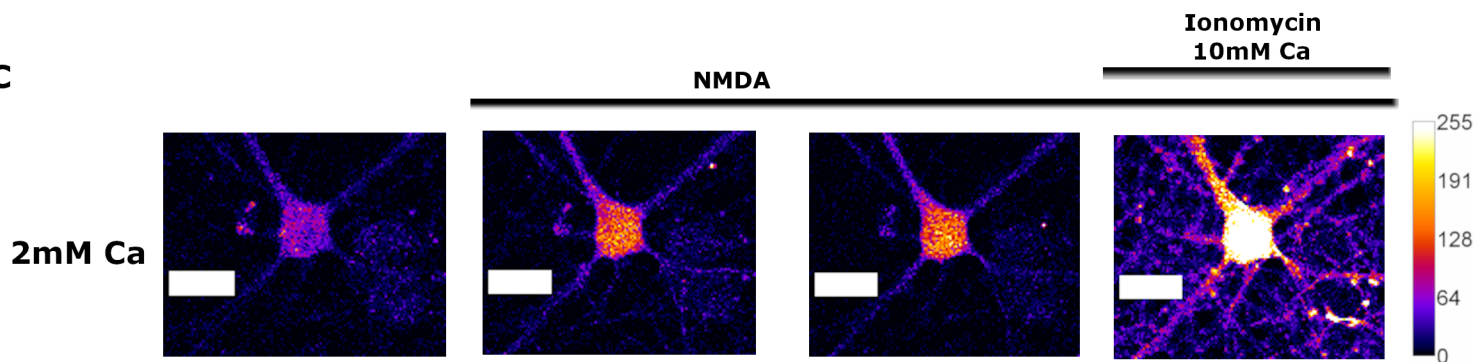
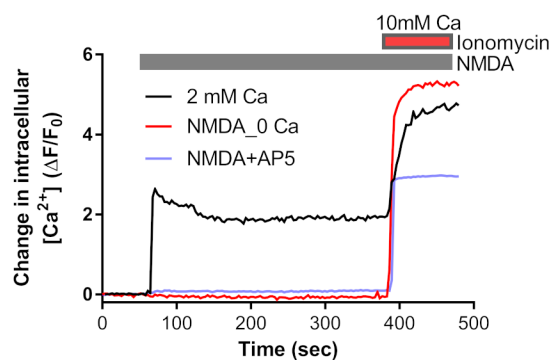
bioRxiv preprint doi: <https://doi.org/10.1101/552638>; this version posted March 30, 2020. The copyright holder for this preprint (which was not certified by peer review) is the author/funder, who has granted bioRxiv a license to display the preprint in perpetuity. It is made available under aCC-BY-NC-ND 4.0 International license.

B**C****D****E****F****G****H**



A

bioRxiv preprint doi: <https://doi.org/10.1101/552638>; this version posted March 30, 2020. The copyright holder for this preprint (which was not certified by peer review) is the author/funder, who has granted bioRxiv a license to display the preprint in perpetuity. It is made available under aCC-BY-NC-ND 4.0 International license.

**B****C****D****E**